

Study of the Localized Nature of Top of the Line Corrosion in Sweet Environment

Marc Singer^{†,*}

ABSTRACT

The phenomena of interest in this study are related to the transportation of gas containing condensable liquids and, more precisely, the corrosion issues that occur when significant heat exchange is present between the pipelines and the surroundings. The unprocessed vapor mixture flowing through the pipe has the potential to condense particular components on the cold walls, one of them being water, forming a thin film and/or droplets of corrosive liquid. In this work, the occurrence of localized corrosion in top of the line corrosion (TLC) was investigated in a sweet (CO₂-dominated) environment, with a focus on understanding the influence of the environmental parameters on localized TLC in order to develop a narrative for the mechanism. A unique setup was developed for the experimental work involving the use of carbon steel inserts exposed to three different levels of cooling at the same time. This concept was quite successful in simulating realistic localized features. A series of long term exposure (1- to 3-month) experiments was conducted to investigate the controlling parameters. The occurrence of localized corrosion could be very clearly correlated to the condensation rate, the gas temperature, and the organic acid content. Additional statistical information related to the morphology of localized TLC features could be collected, providing useful insight on the mechanisms involved. Finally, the very peculiar morphology of typical localized TLC features and the interaction between condensation pattern and corrosion attack were also characterized. However, no clear relationship could be established with certainty between the presence of droplets and the extent of

the corrosion attack. Instead, the water condensation rate (WCR) was thought to control the corrosion and the overall aggressiveness of the environment.

KEY WORDS: condensation, FeCO₃, localized corrosion, top of the line corrosion

INTRODUCTION

When significant heat exchange is present between the wet gas pipelines and the surroundings (frozen land, deep-sea water, etc.), water and hydrocarbon vapor can condense on the inner pipe wall and lead to severe corrosion issues.¹⁻³ This phenomenon, called TLC, is inherently a localized process. Corrosion occurs in specific areas along the line and the attack is not usually extended to large sections. This localized aspect is often related to situations where high condensation rates occur, that is, where the gradient of temperature between the produced fluid and the outside environment is large. In sweet environments (CO₂-dominated), the corrosion process is often characterized as a mesa attack: the steel is not uniformly corroded but the pits are usually wide, often flat-bottomed, and bare of any layers, surrounded by areas with intact corrosion product layers.

A number of field cases attributed to TLC have been reported over the years, most of them encountered in sweet (CO₂-dominated) environments. Gunaltun, et al.,¹ who are among the first authors to identify TLC as a major field issue, describe in great detail a case of CO₂ TLC that occurred in an onshore pipeline in Indonesia.¹ An extensive description of the field parameters as well as a thorough interpretation of the

Submitted for publication: August 8, 2016. Revised and accepted: April 23, 2017. Preprint available online: April 23, 2017. <http://dx.doi.org/10.5006/2222>.

[†] Corresponding author. E-mail: singer@ohio.edu.

^{*} Institute for Corrosion and Multiphase Technology, Ohio University, Athens, Ohio 45701.

underlying causes of corrosion was presented. In-line inspection (ILI) tools were used to identify three locations along the flowline that suffered from extensive internal corrosion on the upper side of the pipe. These three zones corresponded to locations at which the pipe was crossing a river delta, where it was alternately buried and in contact with the flowing water. The CO₂ content in this line was 4.7 mol%, for a total pressure of 90 bars, and the inlet temperature was about 80°C. Considering that the river water was at 25°C on average, this situation led to high local heat exchange with the surrounding environment and consequently high WCRs.

Further analysis completed in 2000 by the Gunaltun, et al.,² showed that the presence of large quantities of acetic acid in the production water accelerated the corrosion rate. Gunaltun, et al., provided more insight into the TLC mechanisms by defining three main zones in the pipeline:

- **The bottom of the line:** At this location, the corrosion can be lowered by the use of inhibitors.
- **The top of the line:** The water vapor condenses and forms droplets attached to the pipe wall. A protective iron carbonate (FeCO₃) layer can be formed in certain cases (in CO₂-dominated environments), but inhibitors cannot reach the top of the pipe and are not effective without pigging or in absence of slugging. Localized corrosion is the predominant form of corrosion.
- **The side of the pipe:** As a result of gravity, the condensed water flows on the sidewall and drains to the bottom. Although the corrosion is also uniform, there is no guarantee that inhibitors could access this location and provide any protection.

The condensation rate was identified as a controlling parameter in TLC. The concept of critical condensation, below which TLC was considered to be manageable, was introduced as an engineering tool. This threshold value was presented as a helpful design tool but could not be expected to be valid under every condition. It was set at 0.25 mL/m²/s, considering that the condensation would happen only on the upper half of the pipe.² If large quantities of organic acid are present (above 2,500 parts per million [ppm] of acetate-containing species), this critical threshold³ is reduced to 0.025 mL/m²/s. Similar observations were made on four separate flowlines located in Europe⁴ and the influence of organic acid was also reinforced.

TLC is now fully recognized as a definitive concern for the industry as a whole.⁵ A large set of results of a field pipeline inspection was presented for a network of offshore pipelines off the coast of Thailand⁶⁻¹⁰ in fields containing high levels of CO₂ (23 mol% on average). The pipelines, ranging from 14-in to 22-in internal diameter, were operated in stratified flow and were only naturally buried on approximately one-third of their surface as the pipes were sitting on the sea bed.

Considering that the inlet fluid temperature could reach 90°C, very high heat exchange with the sea water occurred (on average at 18°C). As the fluid would rapidly cool to ambient, severe water condensation only occurred on the first 500 m of line. TLC was identified as a serious issue leading to potential de-rating of the pipe or replacement of entire sections. Features as deep as 30% to 60% of the original wall thickness were measured by different types of ILI. The deepest features were located in the first 240 m of line, corresponding to the zone of high WCR. The notion of TLC stabilization was also introduced⁹ as consecutive ILI seemed to show that the number and size of the corroded features did not increase with time. However, this observation was based only on highly inaccurate ILI measurements and was therefore uncertain. Nevertheless, valuable information was presented about operating practices and monitoring techniques used in the field to prevent TLC. Several more recent publications related to the same field were published in 2010.¹¹⁻¹² The notion of “cold spot” corrosion was introduced, described as a worst-case TLC scenario. This situation occurred when the pipe thermal insulation had to be removed to accommodate the installation of sacrificial anodes, commonly used for external corrosion. This led to very high local condensation rates, dramatic overall rates of corrosion, and, ultimately, to pipeline failure.

Although there are numerous reported cases of TLC in the field, the localized nature of TLC is still not well understood. The corrosion features observed in the field can be so large that the corrosion process is often referred to as “localized uniform corrosion” instead of just “localized corrosion”. The unique TLC scenario, in which droplets of condensed water appear and are renewed continuously at the metal surface, must play a crucial role. It is likely that the condensation process initiates and promotes the localized corrosion at the top of the line by challenging the protectiveness of the FeCO₃ layer.

There is a clear need to develop a better understanding of the mechanisms of sweet localized corrosion in order to provide more accurate predictions of the likelihood of occurrence and the severity of the attack. This would have direct implications for pipeline design and operation. Conducting cutting edge research is paramount toward achieving this goal but it is also important to develop the right experimental tools. No laboratory setup can perfectly represent the conditions in the field. While pure corrosion issues have been successfully simulated in small scale setups, the flow conditions relative to a 30-in ID pipeline are not easily reproducible.

While several different experimental setups have been used with some success at the Institute for Corrosion and Multiphase Technology (ICMT) at Ohio University and elsewhere, it is believed that significant improvements can be made in the way TLC is simulated.

LITERATURE REVIEW

In the past 20 y, TLC has been the subject of intensive research. This section only focuses on sweet (CO₂-dominated) TLC, as opposed to sour TLC, as it is most relevant to the present study.

Olsen and Dugstad¹³ conducted a systematic experimental study on parameters influencing TLC in sweet conditions. The formation of a protective FeCO₃ corrosion product layer was suggested to play a key role. The precipitation of FeCO₃ only occurs when the saturation level is above the value of one. High levels of super-saturation in FeCO₃ could lead to very dense and protective FeCO₃, as was the case at a high temperature (70°C) and a low condensation rate. The authors also found that the competition between the rate of iron dissolution (i.e., the increase of Fe²⁺ ions in the aqueous phase) and the rate of water condensation controlled the extent of FeCO₃ film formation. At a high condensation rate, the saturation in FeCO₃ was more difficult to obtain because of the rate of fresh water renewal.

In 2000, Pots and Hendriksen¹⁴ conducted a series of experiments aimed at highlighting the competition between the scale formation rate linked to the iron dissolution and the condensation rate. Pots and Hendriksen developed a corrosion prediction model for TLC based on the calculation of the concentration of iron at saturation under film-forming conditions. The author emphasized the importance of correctly evaluating the condensation rate in order to accurately predict the corrosion rate.

In 2002, Vitse¹⁵ and Vitse, et al.,¹⁶⁻¹⁷ completed a thorough experimental and theoretical study on TLC caused by carbon dioxide. Condensation and corrosion experiments were conducted in a large-scale 4 in ID flow loop, which represented a significant improvement on what had been done before. This setup was later upgraded and improved for the purpose of the present study. Vitse and Vitse, et al., were able to link gas temperatures to condensation rates and consequently to corrosion rates at the top of the line. However, Vitse and Vitse, et al., observed that the formation of FeCO₃ was favored by high fluid temperature and could lead to a decrease in the corrosion rate. The experiments also explored the effect of the gas velocity and partial pressure of CO₂ on TLC, which play an important role in the WCR and corrosion rate, respectively. However, the experiments conducted by Vitse and Vitse, et al., were all of relatively short duration (2 d to 4 d) and consequently could not capture the full extent of the corrosion, especially in terms of localized corrosion, which often requires weeks of exposure. Nevertheless, Vitse and Vitse, et al.,'s corrosion model constituted a considerable breakthrough in the understanding of the mechanisms involved in TLC.

Several experimental studies¹⁸⁻²⁰ have been published on the effect of different parameters such as

acetic acid, mono-ethylene-glycol (MEG), or pH control. However, these experiments also had a relatively short exposure time and offered only limited data in terms of localized corrosion. MEG is commonly used in gas fields in order to prevent the formation of methane gas hydrate (a solid ice structure which can obstruct the flow). The presence of a large quantity of MEG (typically 50 wt% to 70 wt%) decreases the water vapor pressure, which effectively inhibits hydrate formation. It also decreases the water condensation because the amount of water vapor is lower. pH control (a method consisting of injecting a base in order to control the bulk aqueous pH) was shown to have no real effect on TLC other than limiting the concentration of undissociated acetic acid in the bulk liquid phase available for evaporation. The presence of acetic acid was found to greatly affect TLC and mild steel corrosion in general.²¹

Okafor and Nestic²² proposed through their experimental study a mechanism for corrosion under liquid droplets containing acetic acid. Okafor linked the initiation of localized corrosion with the presence of protected and non-protected regions under drop-wise condensation. He assumed the formation of a galvanic cell between film-free regions and regions covered by a FeCO₃ film. It was the first attempt to differentiate general and localized corrosion at the top of the line.

Major advances in TLC research were published in 2007. Zhang, et al.,²³ published the first fully mechanistic approach in TLC modeling, covering the three main processes involved in TLC phenomena: dropwise condensation, chemistry in the condensed water, and corrosion at the steel surface. Zhang's approach represents one of the most advanced attempts to model the mechanisms involved in TLC to date. It takes into account all of the most important parameters in CO₂ TLC: condensation rate, gas temperature, CO₂ partial pressure, gas velocity, and acetic acid concentration. Zhang actively participated in the collection of some of the experimental data shown in the present study, and these data were used to validate his model.

Singer, et al.,¹⁸ published the results of an experimental parametric study of sweet TLC performed in 4-in ID flow loops. This study summarized the effect of the most influencing parameters on which the severity of the corrosion attack depends: the condensation rate, the gas temperature, the gas flow rate, the CO₂ partial pressure, and the presence of organic acid. Information about both uniform and localized corrosion was collected through this series of long-term (3-week) experiments. However, issues related to the design of the corrosion samples were identified and, in some cases, led to unwanted edge effects.

In 2011, Rotimi, et al.,²⁴ conducted a series of long-term experiments (up to 6 weeks of exposure) in an autoclave especially designed for TLC study. The effect of water condensation and temperature was

evaluated under different partial pressures of CO_2 . The author reported that the uniform corrosion decreased as the temperature increased, as a result of the formation of a more protective FeCO_3 layer. However, no information was reported on localized corrosion, even though this type of corrosion was expected to play a big role under these conditions.

Since then, several experimental studies have been published on the characteristics of the water chemistry at the top of the line²⁵ and on the possible role of hydrocarbon condensate.²⁶⁻²⁷ It was found that the condensation of light hydrocarbons could not prevent liquid water from reaching the hydrophilic steel surface.

Even though much progress has been made over the years in the understanding of TLC mechanisms, none of the models proposed thus far address the occurrence and prediction of localized corrosion. The first experimental study focusing on this aspect linked to TLC phenomena was published by Amri, et al.,²⁸⁻²⁹ in an effort to relate pit growth and environmental conditions. A conceptual model of pit propagation and growth was proposed, but more validation work was clearly needed because the experimental work was not performed in a setup designed to simulate a representative environment.

RESEARCH OBJECTIVES

As mentioned in Literature Review, because the present understanding of the localized nature of TLC is limited, more work needs to be done to identify the controlling mechanisms. The objectives of the current study are stated as follows:

1. Devise new experimental setups and procedures that can realistically simulate typical TLC (in terms of flow, geometry, corrosive environment, condensation regime) as it is observed in a wet gas pipeline.
2. Investigate the effect of different influencing parameters on TLC (both uniform and localized rates), including the effect of the condensation rate, gas temperature, and concentration of acetic acid.
3. Implement various methods to qualitatively and quantitatively characterize the interaction between condensation pattern and corrosion attack and to define the localized nature of TLC processes.

EXPERIMENTAL PROCEDURES

The experimental setup used for this study has been described elsewhere^{18,30} and only original aspects are presented as follows.

The experiments were performed in a high-temperature, high-pressure, 4-in ID (0.1-m internal diameter) flow loop (Figure 1). The flow loop is

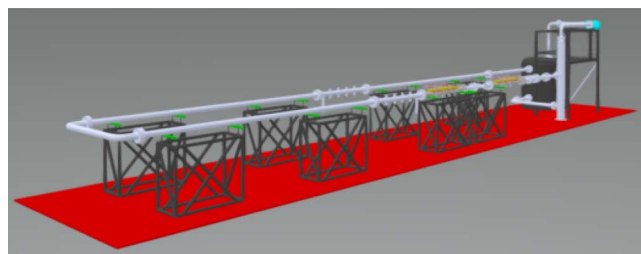


FIGURE 1. Schematic of the wet gas flow loop.

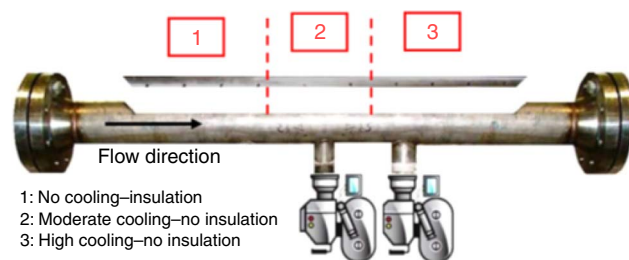


FIGURE 2. Flat slab cooling setup.

comprised of a large tank (1,000 L) holding the bulk liquid phase, a gas blower (and in some cases a liquid pump), and a system of 4-in ID (0.1-m internal diameter) stainless steel pipes forming a loop. The system is about 30 m in total length. Various monitoring devices (pressure gauge, thermometers, gas flow meter, liquid sampling device) are installed along the pipe system. Several test sections, where the actual corrosion measurements are performed, are located along the pipe system.

The test section utilized for this study was derived from the “flat slab” concept aiming at simulating the large pipe curvature of a 30-in ID (0.76-m internal diameter) pipeline—a size commonly encountered in oil and gas fields—which is much closer to a flat surface than the 4-in ID pipe. A portion of a pipe section was especially manufactured in order to enable the insertion of a thick, flat stainless steel slab about 1 m long (Figures 2 and 3). The stainless steel slab and the pipe were sealed together using a thermally resistant silicon resin. On top of the stainless steel slab lay an aluminum slab containing a cooling system that enabled the control of the condensation rate. A set of thermistors embedded in the stainless steel component was used to monitor the steel temperature and compute the condensation rate on each section. The condensation rate was determined by measuring the difference in temperature between the gas and the pipe wall’s inner surface using a model developed by Zhang, et al.²³

A carbon steel bar of the approximate dimensions 2 in \times 1/4 in \times 37 in (0.05 m \times 0.006 m \times 1 m) acted as the corrosion specimen and was then mounted into the stainless steel slab using spring loaded set screws (Figure 3). Prior to mounting, it was coated with

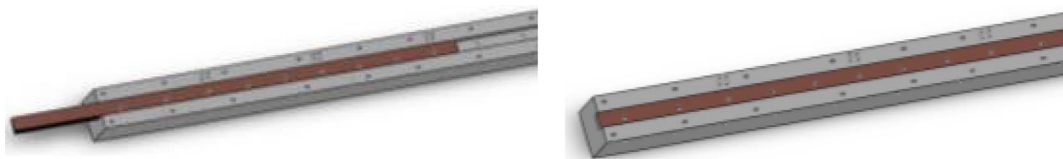


FIGURE 3. Design of the carbon steel insert in stainless steel slab.

polytetrafluoroethylene on the outer edges and bottom surface in order to electrically isolate the carbon steel bar from the slab. The uncovered steel surface was then polished with 600-grit silicon carbide paper wetted with isopropanol, cleaned, and dried. Three 20-cm long zones with different cooling areas were created (Figure 2): A well-insulated section (1), a section not insulated but not subject to forced external cooling (2), and a section subject to high external cooling (3). At the end of the test, the carbon steel insert was sprayed with water and dried with alcohol as soon as the system was depressurized and open to atmosphere.

Another design similar to the one shown in Figure 3 was used for some of the tests and enabled the use of cylindrical steel samples (instead of a carbon steel bar) flushed to a stainless steel flat slab. It enabled the collection of corrosion rates in addition to the analysis of the steel surface of the samples. However, it also suffered from unwanted edge effect, as the samples could not be perfectly flushed with the slab surface. The full description of this setup is shown elsewhere.³⁰

Information on the occurrence and extent of localized corrosion was collected for each test using a 3D surface profilometer. The results of a line profile (measuring the depth of features along selected line) were used to determine the rates of localized corrosion, which were calculated by dividing the feature depth (the average or maximum pit depth) by the exposure time; these are shown in mm/y. Information about the percentage of the steel surface area affected by localized corrosion was also obtained using a mapping tool enabling a statistical analysis of the data.

The carbon steel inserts used in the “flat slab” test section were obtained from two different batches of UNS 1018⁽¹⁾ carbon steel. Later on, a 20-in ID (0.5 m internal diameter) API 5L X65 section of pipe was obtained, and all new steel inserts were made from this source. The chemical composition analysis, showing very similar composition within the specification of UNS 1018 or API 5L X65, is shown in Table 1. All three samples present a ferritic-pearlitic microstructure, consisting of a mixture of ferrite (white constituent), and pearlite colonies (black constituent). However, the steel samples present differences in microstructure as it relates to the volume fraction, colony site, and colony

TABLE 1

Chemical Composition of Steel Samples Used in the Experiments. C1018 Steel Insert (I) for Test No. 1, (III) for Test No. 2 and API L X65 for Test Nos. 2 and 3

Element	Min	Max	(I)	(III)
C	0.15	0.2	0.19%	0.19%
Cr			0.069%	0.07%
Cu			0.021%	0.022%
Mn	0.6	0.9	0.74%	0.75%
Mo			0.024%	0.024%
Ni			0.11%	0.116%
P		0.03	0.017%	0.018%
S		0.05	0.014%	0.016%
Si			0.012%	0.012%

Element	Min	Max	X65
C	0.1	0.16	0.14%
Mn	1.1	1.4	1.39%
P		0.04	0.008%
S		0.05	0.008%
Si			0.36%

density of the pearlite constituent.³⁰ Nevertheless, no difference in corrosion mechanism could be observed.

When required, the organic acid was introduced as glacial acetic acid directly in the bulk liquid phase in the tank. The quantity of acid introduced was calculated based on the measured initial bulk pH in order to reach the target concentration of undissociated acetic acid. During the experiment, the bulk pH increased gradually over the 3 months of testing, from 3.8 to 4.5. Consequently, the concentration of undissociated acetic acid also gradually decreased from 1,042 ppm, initially, to 750 ppm at the end of the experiment. For clarity reasons, the acetic acid concentration is referred to as 1,000 ppm for the rest of the publication.

In addition, a novel high-pressure, high-temperature video camera was acquired for this study in order to enable direct observation of the condensation and the corrosion processes (<http://www.envirocam.net>). The video camera was especially designed to be mounted on the test section using one of the bottom ports. Live visual observation of the condensation process occurring on the corresponding top port was consequently rendered possible. Under the conditions investigated in this study (low gas velocity and low pressure), the droplets of condensed liquid that formed on the steel surface grew by condensation and

⁽¹⁾ UNS numbers are listed in *Metals and Alloys in the Unified Numbering System*, published by the Society of Automotive Engineers (SAE International) and cosponsored by ASTM International.

then eventually reached their maximum size and underwent detachment from the metal surface as a result of gravity forces.

RESULTS

The experimental results and Discussion section are divided into three main parts:

- The first part, labeled “Corrosion Study,” presents a summary of the most relevant experimental work performed with the new “flat slab” concept.
- The second part, “Direct Observation of the Condensation process,” discusses the implementation of various methods and qualitatively and quantitatively characterizes the interaction between condensation pattern and corrosion attack.
- The third part, “Characteristics of localized features at the top of the line,” investigates the very peculiar morphology of typical localized TLC features in order to gain insight into how localized corrosion is initiated and how it progresses.

More details can be found in the author’s dissertation.³⁰

Part 1: Corrosion Study

The test matrix (Table 2) was selected in order to investigate the effect of the water condensation using the experimental setup described under Experimental Procedures. The tests were all performed at $p\text{CO}_2 = 2.7$ bars (no H_2S), under stratified flow regime and for a duration of 3 months each. The varied parameters were the gas temperature (65°C, 45°C, and 25°C) and the organic acid concentration (0 ppm and 1,000 ppm of undissociated CH_3COOH). Although three WCRs were applied for each test, their specific values differed for each condition because of their dependence on the gas temperature. The results of each test are first presented individually, and a discussion is proposed at the end of the section.

Test No. 1: $T_{\text{gas}} = 65^\circ\text{C}$ — An inspection of the corrosion product was performed immediately after the end of the test and the retrieval of the carbon steel sample. The part of the steel insert exposed to a low condensation rate (0.12 $\text{mL}/\text{m}^2/\text{s}$ to 0.15 $\text{mL}/\text{m}^2/\text{s}$) did not seem to be highly corroded (i.e., the corrosion product layer was still fairly intact). The part of the insert exposed to a high condensation rate (0.76 $\text{mL}/\text{m}^2/\text{s}$ to 0.95 $\text{mL}/\text{m}^2/\text{s}$) seemed much more affected by corrosion. Numerous failures of the corrosion product layer (which is usually related to extensive localized corrosion) could be observed, especially on the section exposed to higher WCRs. A yellow/orange color found on part of the steel sample is a sign of the presence of iron oxide (most likely ferric oxide [Fe_2O_3]), which is thought to have formed after

TABLE 2

Localized Condensation/Corrosion Study—Test Matrix^(A)

Test #	1	2	3	4
Investigating	Gas temperature			CO ₂ /HAc
Steel type	C1018(I)	X65	X65	C1018(III)
T _g (°C)	65	45	25	65
Initial Undissociated HAc (ppm)	0	0	0	1000
Low WCR ($\text{mL}/\text{m}^2/\text{s}$)	0.13	0.1	0.04	0.2
Medium WCR ($\text{mL}/\text{m}^2/\text{s}$)	0.41	0.15	0.06	0.4
High WCR ($\text{mL}/\text{m}^2/\text{s}$)	0.9	0.23	0.1	0.7

(A) Test duration: 3 months; Gas velocity: 2.5 m/s - $p\text{CO}_2 = 2.7$ bars - $p\text{H}_2\text{S} = 0$ bar - PT= 3 bars.

the end of the experiment as the slab assembly was removed from the loop. Operational procedures often require a few minutes before the steel insert, wetted by droplets of condensed water saturated with species generated as a result of corrosion processes, can be accessed and dried. In this elapsed time, the steel is exposed to air. During the experiment itself, great care is given to maintain the level of oxygen in the bulk liquid phase below 20 ppb so as not to interfere with the corrosion process.

The scanning electron microscope (SEM)/energy dispersive spectroscopy (EDS) analysis of the corrosion product layer showed that no significant difference in type and composition was observed with regard to the change in WCRs. Although no x-ray diffraction (XRD) analysis was performed, the corrosion product layer is believed to be a mixture of FeCO_3 and iron oxide. Once again, the iron oxide must have formed during the removal of the slab assembly at the end of experiment. Some crystals of FeCO_3 could be seen underneath the Fe_2O_3 layer.

These initial observations were confirmed with the surface analysis on the bare steel shown in Figures 4 through 6 (once the corrosion product layer was removed using an inhibited acid solution³¹). The section of the insert exposed to a low condensation rate did present some pitting corrosion, but the pits were fairly isolated. In the middle section exposed to a medium condensation rate (not shown in this publication), the pitting density increased. The pits seemed to coalesce in the section exposed to a high condensation rate, which also showed severe mesa attack (localized corrosion with flat bottom features). The relationship between condensation rate and localized corrosion is, therefore, clearly demonstrated in this experiment. These corrosion features very much resemble what is observed in real field situations.¹

Average, minimum, and maximum localized corrosion rates were extracted from the 3D profile analysis of selected areas thought to be representative. The localized corrosion data are presented in Figure 7(a) and compared to experimental data obtained under the same conditions but for an exposure time of 21 d.¹⁸ The “21-day” experimental data were

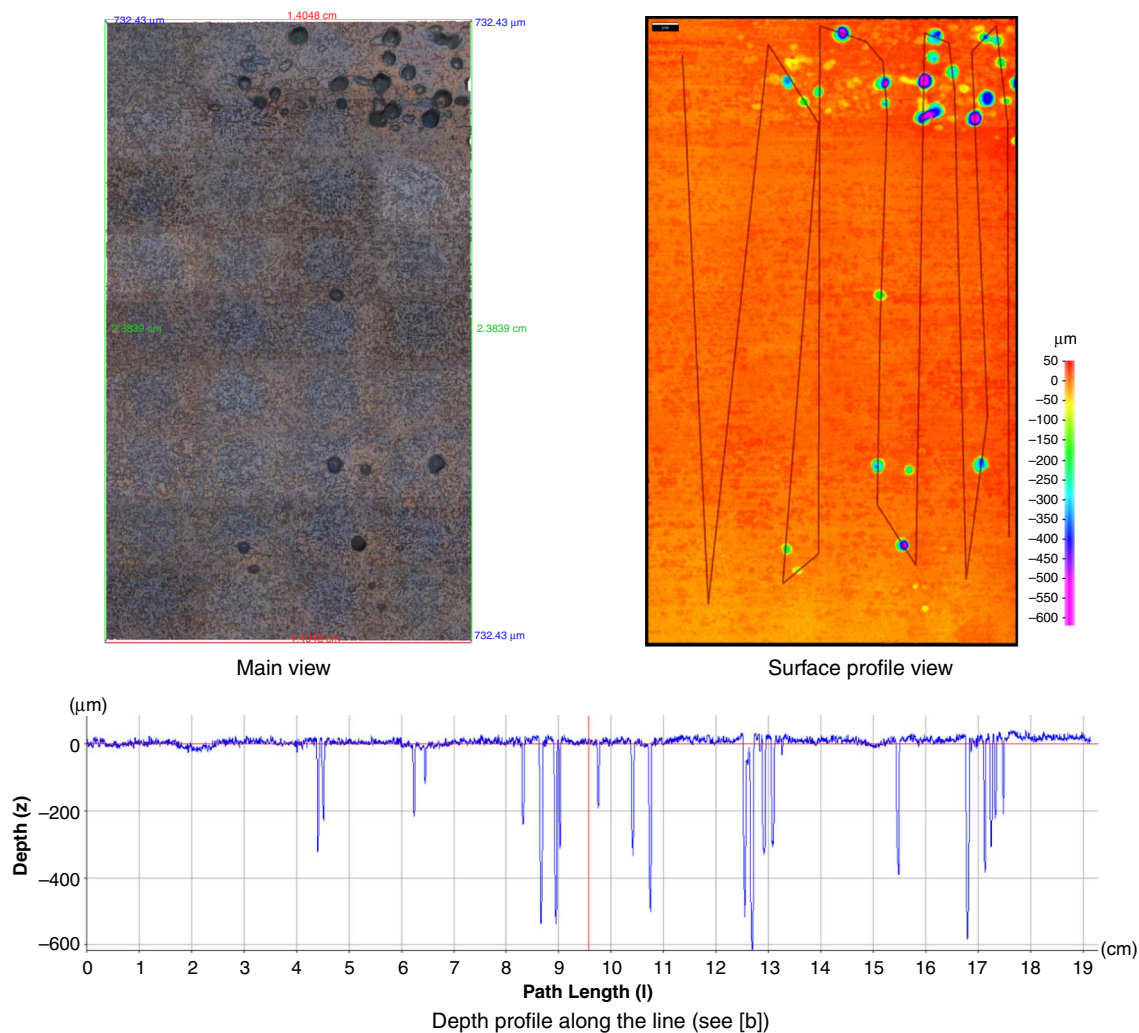


FIGURE 4. Test No. 1: 65°C—Surface profile analysis. Upstream section—Low condensation (0.13 mL/m²/s).

obtained by performing a surface profile scan on weight loss samples. Comparing the data obtained after 21 d and 93 d of exposure, the localized corrosion rates (or more accurately—the steel penetration rates) clearly increase with the WCR but also decrease with time. Another way to compare the two sets of data is to plot the actual feature depth versus the condensation rate (Figure 7[b]). It is interesting to note that at condensation rates lower than 0.4 mL/m²/s, the average feature depth after 21 d and 93 d of exposure is very similar. It could mean that the pit or mesa attack penetration rate significantly slowed down after 21 d of exposure. At a condensation rate of 1 mL/m²/s, the localized attack depth measured after 93 d of exposure is almost 50% higher than the one measured after 21 d of testing. The hypothesis here is that TLC may have significantly slowed down at a condensation rate below 0.4 mL/m²/s, while it did not at a condensation rate of 1 mL/m²/s. This is in some ways consistent with field observations, noting the existence of a “threshold” WCR in sweet environments below which TLC is not

a lasting issue.² The maximum feature depths do show the same trend, although the “threshold” WCR seems to be much lower.

The percentage area affected by localized corrosion could also be measured on the steel surface; the results are displayed in Figure 8 and compared with data obtained for 21 d of exposure. It is clear that, with time, a higher proportion of the steel surface area is corroded when the WCR is high. Again, this is in agreement with field observations, which seem to show that, although TLC corrosion features’ depth may not progress at a fixed rate, their numbers do increase with time.⁷ As the features grow in number, they coalesce, and the steel surface becomes more uniformly attacked. This is clearly demonstrated by the data collected in Figure 8, which shows the number of pits per surface area increasing with condensation rate, together with the average feature diameter. The maximum depth of the feature does increase as well, but to a lesser extent.

Test No. 2: $T_{gas} = 45^{\circ}\text{C}$ —A second experiment was conducted at a lower temperature (45°C instead of

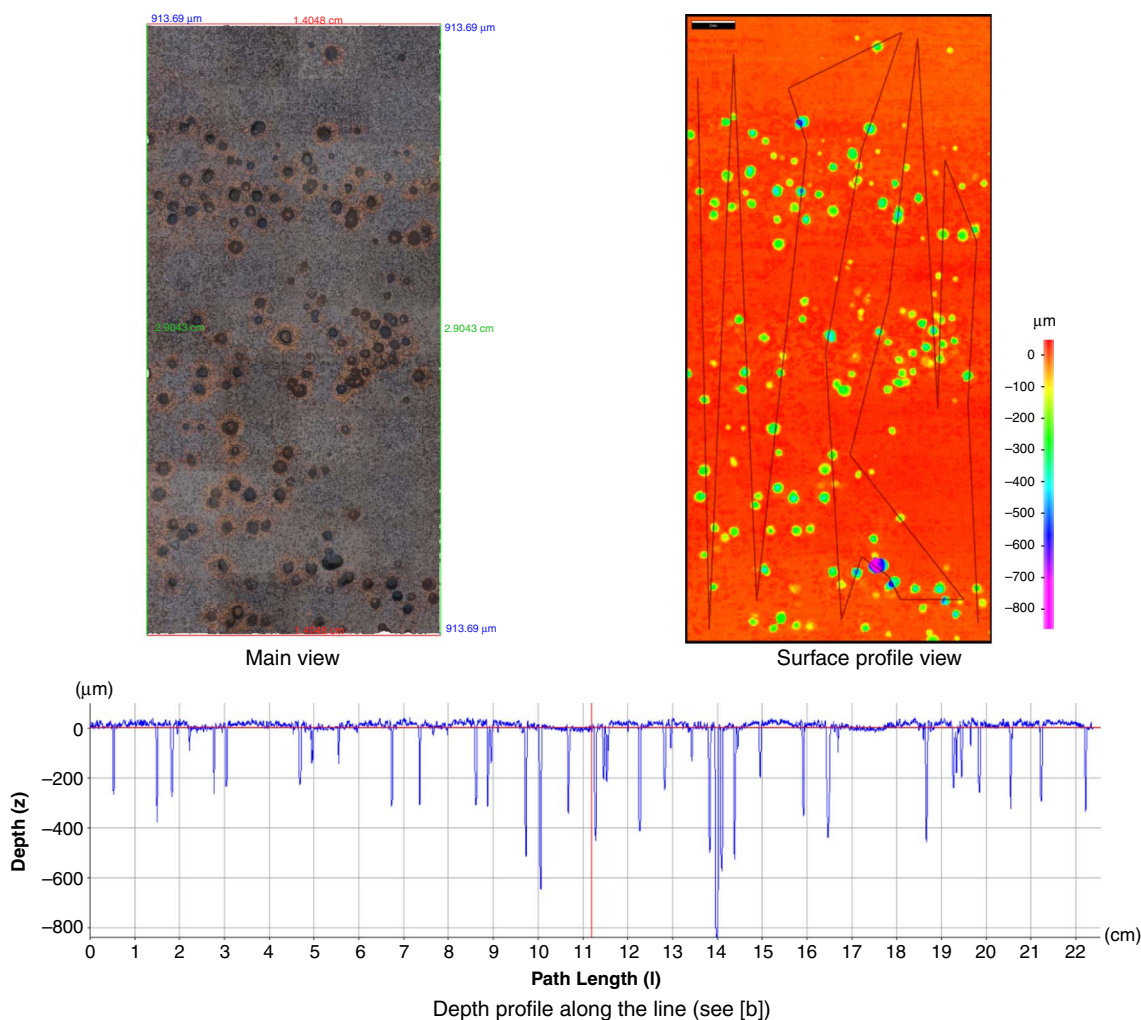


FIGURE 5. Test No. 1: 65°C—Surface profile analysis. Middle section—Medium condensation (0.41 mL/m²/s).

65°C). The primary objective was to investigate the range of test conditions (mainly temperature and WCR) for which FeCO₃ formation and localized corrosion would be encountered in a TLC scenario.

The initial observation of the state of the slab immediately after the test showed that the extent of corrosion seemed higher on the part exposed to higher WCR. More cracks in the corrosion product layers were observed on the cooled section, which is usually synonymous with higher corrosion rate. As for the previous test, some iron oxide (most likely Fe₂O₃) was also present on the steel surface but is thought to have appeared during the slab removal process, which can take several minutes.

The SEM/EDS analysis was performed on different sections of the insert, but no major difference was observed as a result of the level of cooling. The corrosion product layer was made of a mixture of FeCO₃, iron carbide (Fe₃C), and iron oxide. Most of the steel surface was covered with FeCO₃, while Fe₃C could be found inside cracks in the FeCO₃ layer, as is commonly the case in a TLC scenario.

The surface of the steel insert was analyzed after removal of the corrosion product layer using inhibited acid. The cooled section was clearly more affected by pitting corrosion than any other part, as anticipated. However, the extent of TLC was more severe than expected at this lower temperature. Previous testing performed with weight loss samples showed no localized corrosion and low/moderate uniform corrosion at the top of the line at a gas temperature of 40°C.¹⁸

Large areas of the steel slab were scanned using a 3D surface profilometer, and data on pit depth were collected (Figures 9 and 10). The effect of the condensation rate is clear, as the number of pits and the area affected by localized corrosion rate increased with the condensation rate.

Test No. 3: T_{gas} = 25°C—A third experiment was conducted at an even lower temperature (25°C). The expected result was to find mostly uniform corrosion at the high range of WCRs.

Preliminary observation of the state of the insert immediately after the end of the test (before removal of

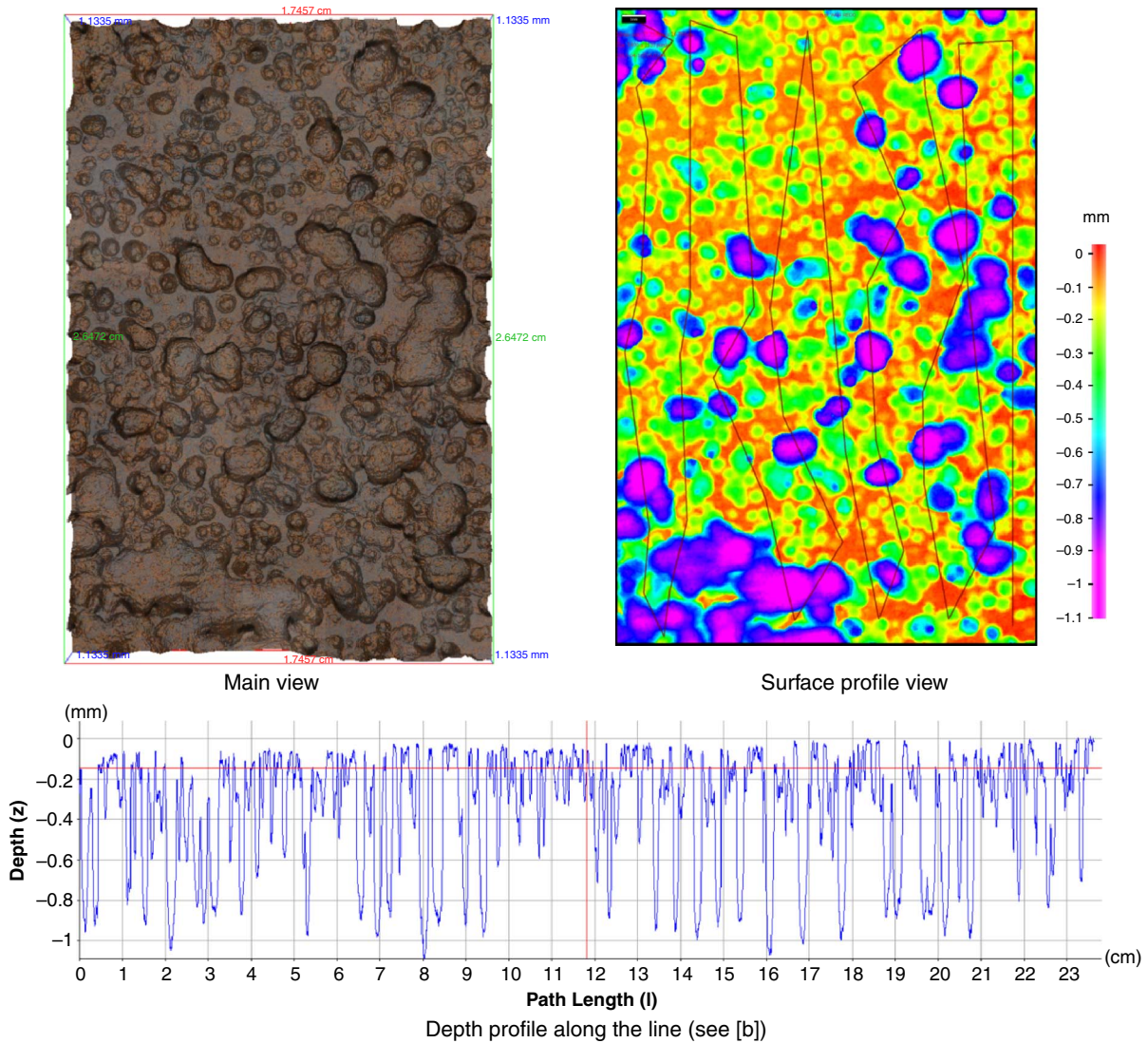


FIGURE 6. Test No. 1: 65°C—Surface profile analysis. Downstream section—High condensation (0.9 mL/m²/s).

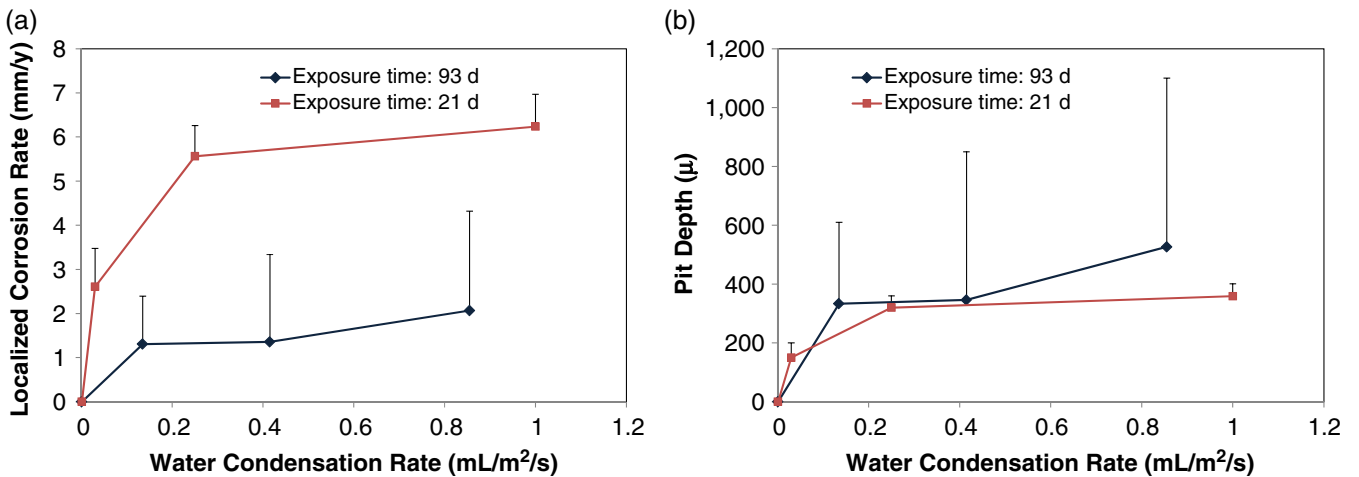


FIGURE 7. Test No. 1: 65°C. Left: Influence of the condensation rate on the localized corrosion rate. Right: Influence of the condensation rate and the exposure time on the pit/mesa depth.

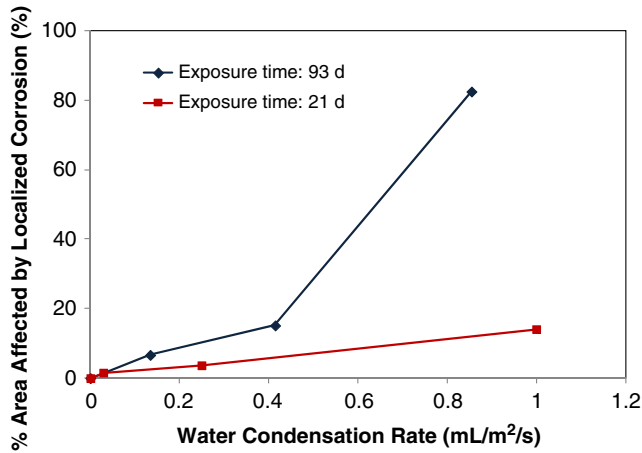


FIGURE 8. Test No. 1: 65°C—Influence of the condensation rate on the percentage of the steel surface area affected by localized corrosion.

the corrosion product layer) shows that the corrosion product uniformly covered the surface of the steel exposed to low condensation rate. However, a very loose and poorly adherent layer covered the section of the insert exposed to higher WCR (0.1 mL/m²/s). The layer appeared to have formed large flakes, and most of it fell off the steel surface as the slab was being prepared for post-processing and analysis. The “bare” steel surface underneath appeared to be uniformly corroded.

As expected, the SEM/EDS analysis of the corrosion product was consistent with FeCO₃. No other corrosion product layer could be expected in the range of pH and potential encountered in the study. Fe₃C was observed on some areas of the steel insert but this type of layer is more an indicator of high corrosion rates and exists under any experimental conditions.

Analysis of the steel surface after the removal of the corrosion product layer showed widespread localized corrosion of the middle section, exposed to a condensation rate of 0.06 mL/m²/s. The upstream

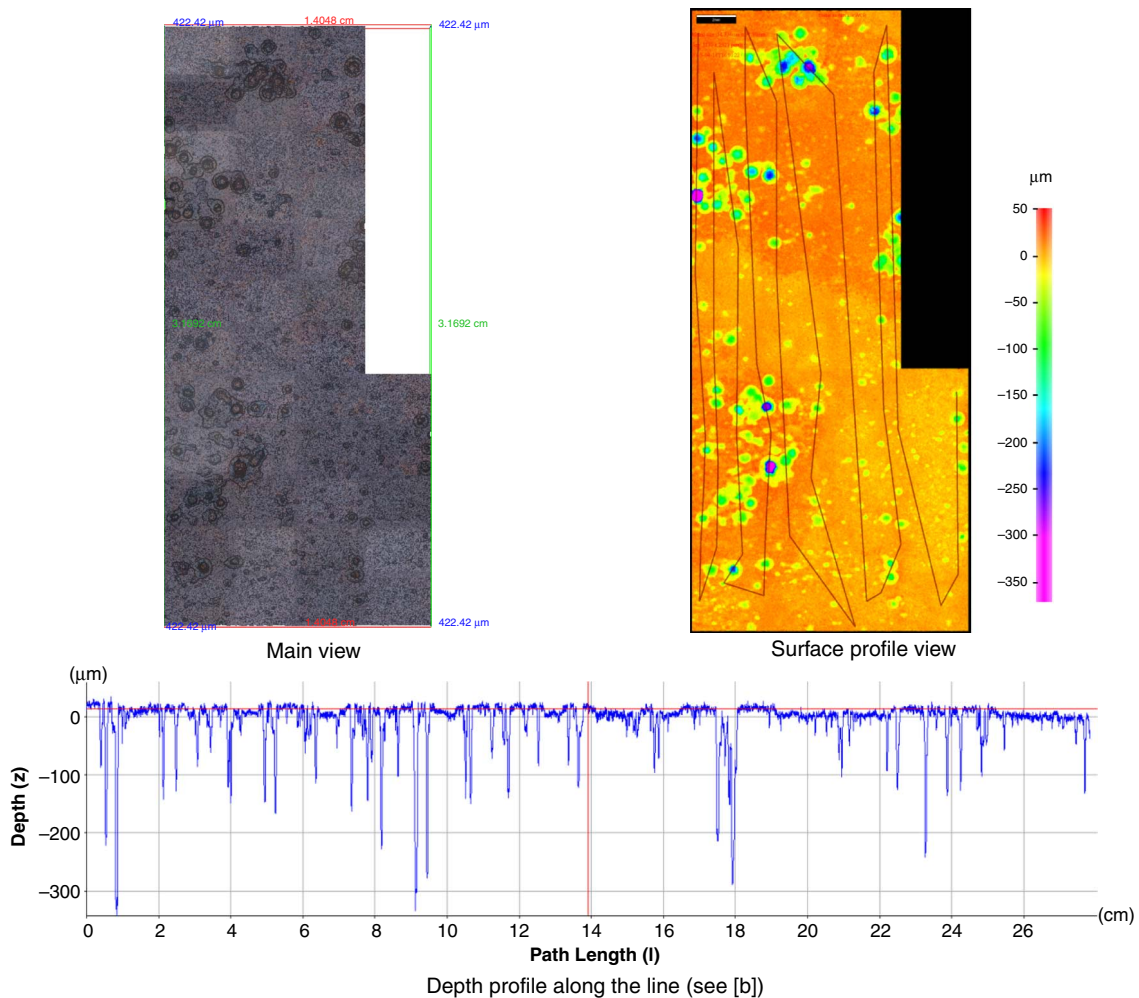


FIGURE 9. Test No. 2: 45°C—Surface profile analysis. Upstream section—Low condensation rate: 0.1 mL/m²/s.

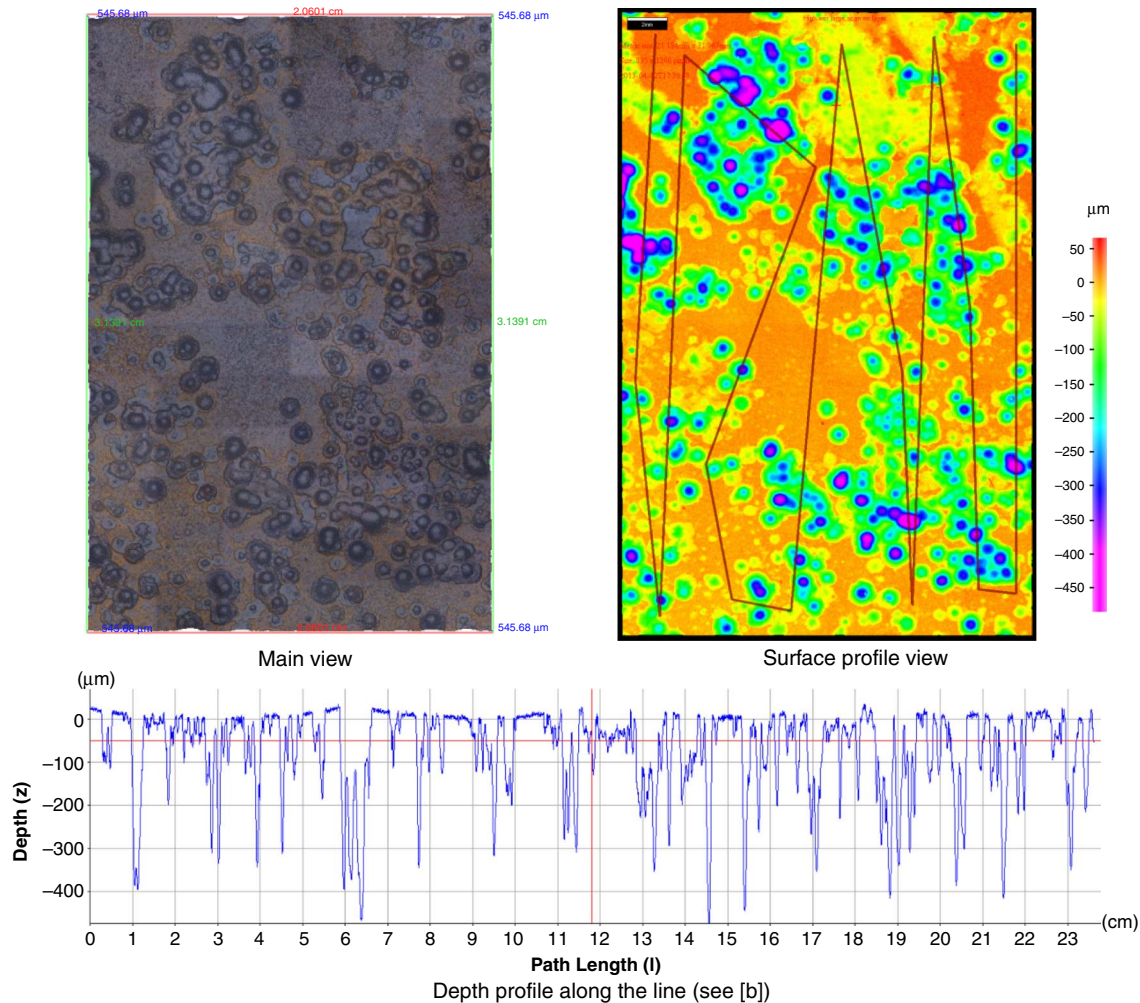


FIGURE 10. Test No. 2: 45°C—Surface profile analysis. Downstream section—High condensation rate: 0.23 mL/m²/s.

area, exposed to the lowest WCR, experienced limited localized corrosion. On the other hand—and contrary to the previous “steel insert” experiments—no sign of localized corrosion could be found on the area of high WCR.

Large areas of the insert were scanned using a 3D surface profilometer, and data on pit depth were collected (Figure 11). The extent of localized corrosion clearly increased with the WCR, but only up to a certain limit (between 0.06 mL/m²/s and 0.1 mL/m²/s in this case). At the highest WCR tested, the steel surface was evenly corroded and no trace of localized corrosion could be found. The 3D surface profilometer data are plotted with the condensation rate in Figure 12. Localized corrosion is only sustainable in the presence of a semi-protective corrosion product layer (here FeCO₃), provided that this layer is adherent to the metal surface and can provide protection on some part of the steel surface. At high WCR (>0.1 mL/m²/s), the corrosion product layer does not adhere to the metal surface and the corrosion can consequently only be uniform in nature.

Test No. 4: Influence of the Presence of Acetic Acid— A final experiment was performed in order to investigate the effect of a high content of organic acid on TLC under high gas temperature and high WCR conditions.

Photographs of the steel insert were taken immediately after the end of the test. A thin layer of iron oxide covered most of the steel surface but was believed to have formed during the process of removal of the flat slab. The oxide layer was, however, very thin and superficial; it would flake off very easily, leaving behind a gray layer, expected to be FeCO₃.

The SEM/EDS analysis of the corrosion product film was performed on the different sections of the insert. There was no major variation in the film characteristics between the sections exposed to different condensation rates. The corrosion product layer is believed to be a mix of iron oxide (most likely Fe₂O₃), FeCO₃, and Fe₃C.

The surface profile analysis was performed on the steel samples after the removal of the layer (Figures 13 and 14). The extent of the corrosion on the

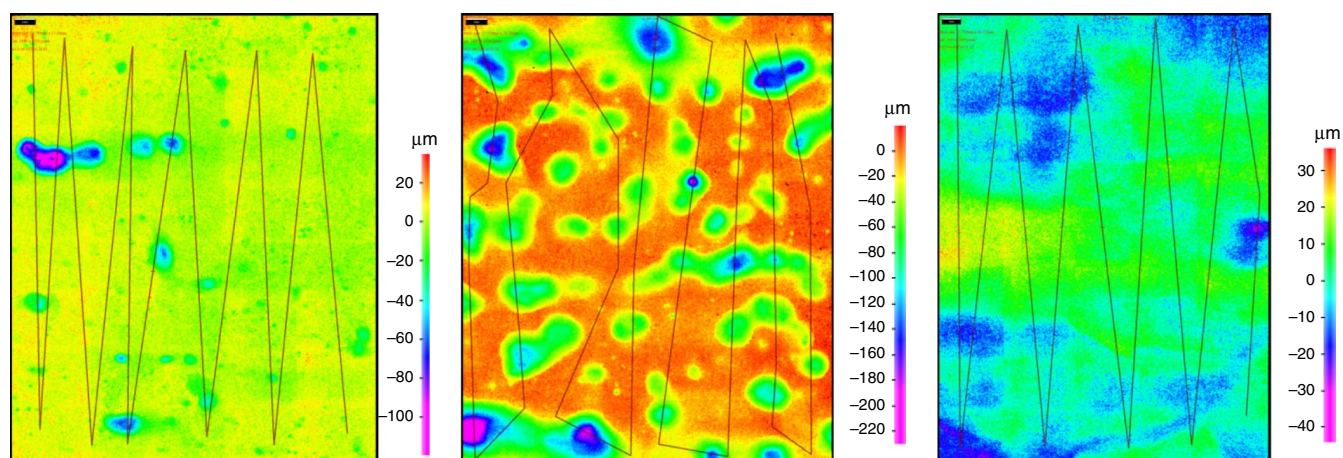


FIGURE 11. Test No. 3: 25°C—Surface profile analysis after the removal of the corrosion product layer. Left: Upstream section—Low condensation ($0.04 \text{ mL/m}^2/\text{s}$). Middle: Middle section—Medium condensation ($0.06 \text{ mL/m}^2/\text{s}$). Right: Downstream section—High condensation ($0.1 \text{ mL/m}^2/\text{s}$).

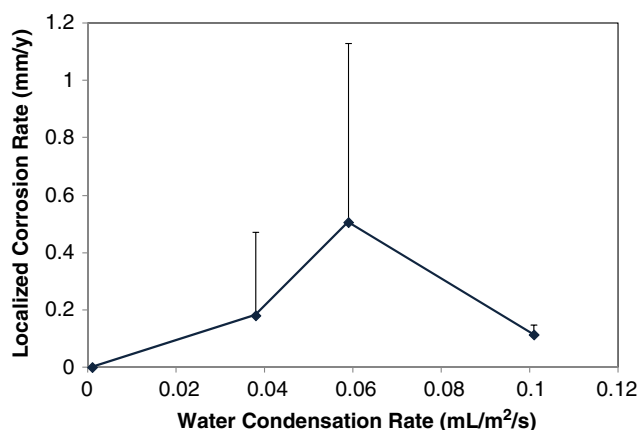


FIGURE 12. Test No. 3: Influence of the condensation rate on the pit/ mesa depth.

downstream section exposed to the highest condensation rate was impressive. The upstream section seemed much less affected, but in all cases pits were measured at similar maximum depths ($800 \mu\text{m}$ to $1,200 \mu\text{m}$). Pits became more numerous as the condensation rate increased and tended to agglomerate together and constitute mesa attack. Large areas of the steel insert were scanned using a 3D surface profilometer, and data on pit depth were collected.

Comparison between the pit depth results obtained for the short term experiments performed with weight loss samples under similar conditions showed that, as for Test No. 1, the localized corrosion rates (or more precisely the steel penetration rates) were about four times lower after 99 d of exposure as compared to 21 d of exposure. The presence of acetic acid did not modify the overall trend although the feature depth was significantly higher, as shown in the next section.

DISCUSSION

Additional feature characteristics could be extracted from the 3D profile analysis, and an effort to collect statistical data for the pit depth distribution is presented in this section. The following values were systematically computed:

- the average and maximum feature depth and corresponding localized corrosion rates;
- the average feature diameter (assuming a cylindrical shape);
- the pitting density (number of pits per unit area); and
- the percentage area affected by localized corrosion.

Additional statistical parameters were collected and correlated to the morphology of the localized features.

The arithmetic mean μ calculates the average depth of features with the top steel surface as a reference. The closer the arithmetic mean is to zero, the lower is the extent of localized corrosion, in terms of depth and number of features.

The standard deviation σ shows how much variation exists from the mean. High standard deviation indicates that the feature depth is spread out over a wide range of values.

The root mean square (RMS) is a representation of the magnitude of the variation in pit depth over the entire surface area. A low RMS number means that the corrosion features are either shallow or very few in numbers. In the case of this study, a higher RMS number is an indication of a higher number of deeper pits.

The skewness and kurtosis factors are used to characterize the shape of a distribution of feature depths over the entire steel surface. The tallest bar on

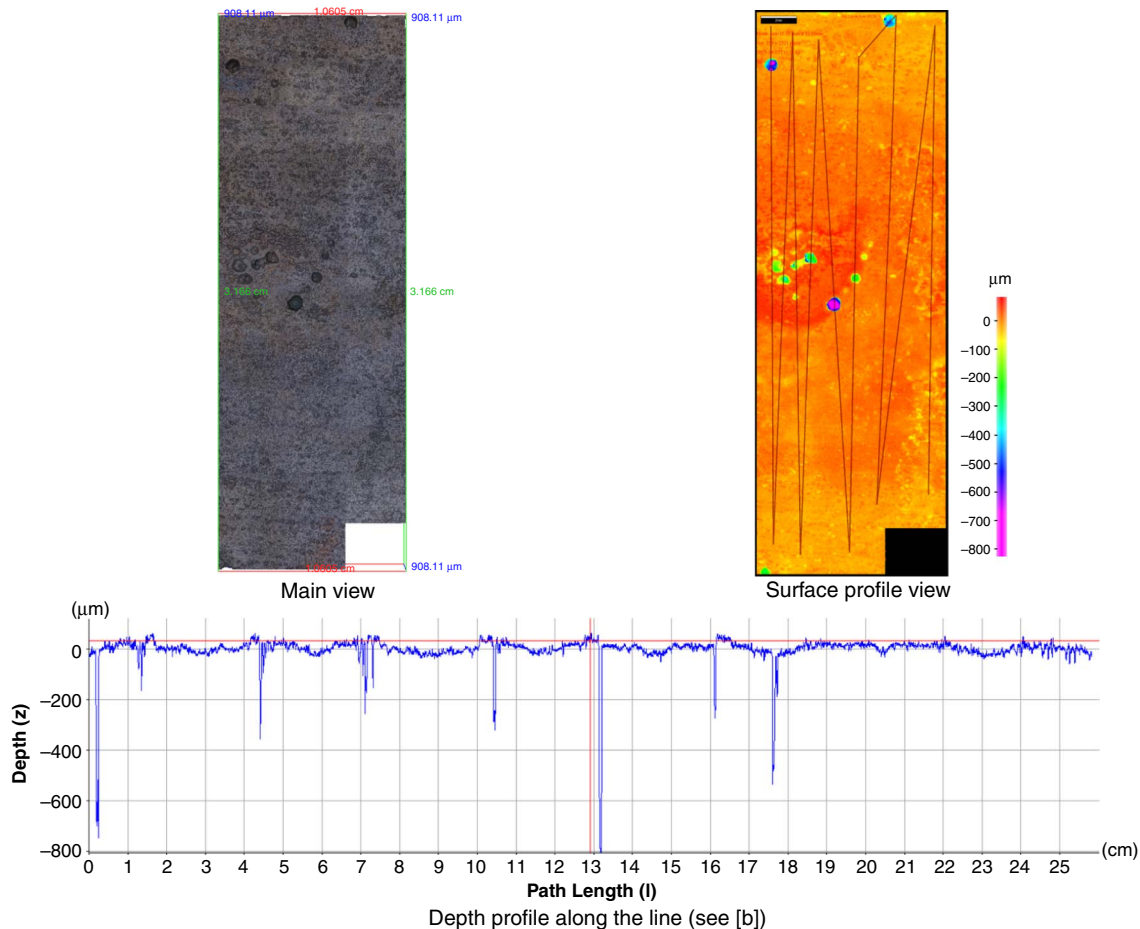


FIGURE 13. Test No. 4: 1,000 ppm CH_3COOH —Surface profile analysis. Upstream section—Low condensation rate: $0.2 \text{ mL/m}^2/\text{s}$.

the distribution always expresses the percentage of surface area at the “zero” or “reference” level (top surface). The skewness represents the extent to which the distribution leans to the left of this reference plan. Skewness values are consequently negative in this case because the tail of the distribution is almost always longer on the left side. A high absolute value of skewness is obtained when deep isolated pits are present on the metal surface (long and thin left tail). To the other extent, a skewness of zero is obtained when the surface is perfectly symmetrical (for example, in the case of uniform corrosion) and when there is absolutely no pit. The kurtosis is a representation of the peak characteristics (width of the peak) and tail weight. It is always a positive number that approaches zero as the distribution becomes flatter. For isolated, deep pits, the kurtosis factor will be high. Heavily pitted surfaces, where the distribution tail is thick, will have lower kurtosis factors.

Effect of Temperature

This section presents a comparison of the experimental results obtained at different gas

temperatures (65°C, 45°C, and 25°C). The tests were performed without acetic acid.

Figure 15(a) shows the effect of the water condensation on the localized corrosion rates. The WCR depends on the gradient of temperature between the outside environment (steel surface) and the bulk gas. Consequently, the effect of water condensation and steel surface or gas temperature cannot be treated separately. The following comments are made:

- Low WCR is often associated with high steel surface temperature (small gradient of temperature) and leads to the formation of an adherent and protective FeCO_3 layer. At very low gas temperature, kinetics of FeCO_3 formation are not favored, but supersaturation is still easily reached because of the relatively low rate for condensed water renewal. FeCO_3 can precipitate, and pits can initiate but do not seem to progress with time.
- High WCR is often associated with lower steel surface temperature (larger gradient of temperature). Two sub-cases are then identified:

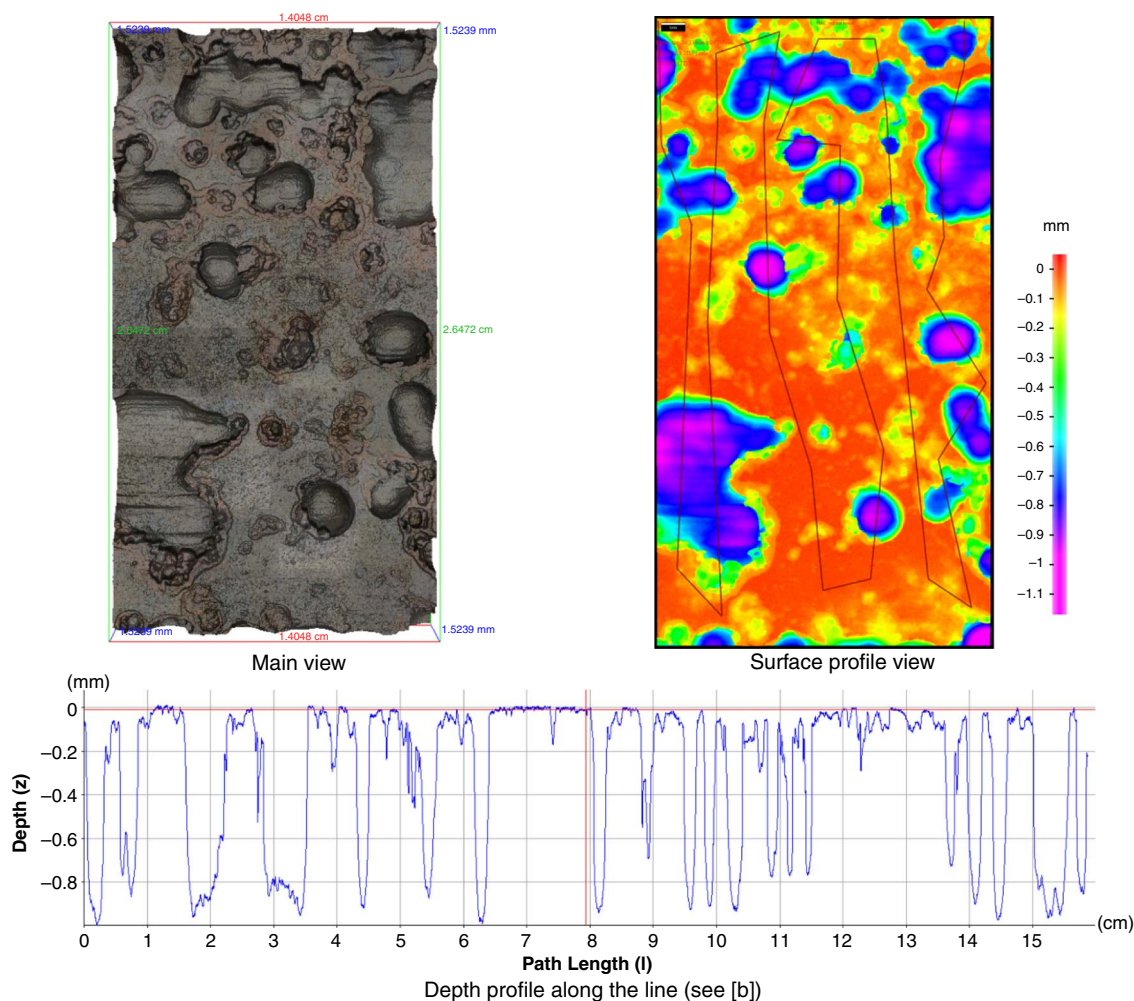


FIGURE 14. Test No. 4: 1,000 ppm CH_3COOH —Surface profile analysis. Downstream section—High condensation rate: $0.7 \text{ mL/m}^2/\text{s}$.

- If a partially adherent/protective FeCO_3 layer forms (as a result of moderate steel temperature), localized corrosion is initiated and can be very severe.
- If the steel temperature is too low to form an adherent corrosion product layer, localized corrosion cannot be initiated and the corrosion is uniform.
- At lower gas temperature, high WCRs are difficult to achieve, as the water vapor pressure is lower. However, for a fixed WCR, the average and maximum localized corrosion rates are only marginally higher at higher temperature.

The main influence of the gas temperature is seen in the percentage area affected by localized corrosion, which increases very rapidly with WCR at lower temperature (Figure 15[c]). The corrosion attack switches from localized to uniform over a small variation of condensation rates. This is reflected by an increase in FeCO_3 solubility at low temperature and

the difficulty of forming an adherent and protective corrosion product layer. The maximum feature diameter is similar under all conditions tested but the features will be correspondingly deeper at higher temperatures (Figure 15[a] and [e]). There is also a logically greater variation in the feature depth distribution at higher temperature (Figure 15[d]) because the features are often deeper and more isolated than at lower temperatures.

Influence Of The Presence Of Acetic Acid

This section presents a comparison of the experimental results obtained at different acetic acid concentrations (0 ppm and 1,000 ppm). Statistical parameters are consistent with a wide variation in corrosion feature depth, especially at high WCRs (Figure 16[b]) and the presence of deep but isolated pits at lower WCR (Figure 16[f]). The main effect of the presence of acetic acid is seen at high WCR on the average feature diameter and the percentage area of

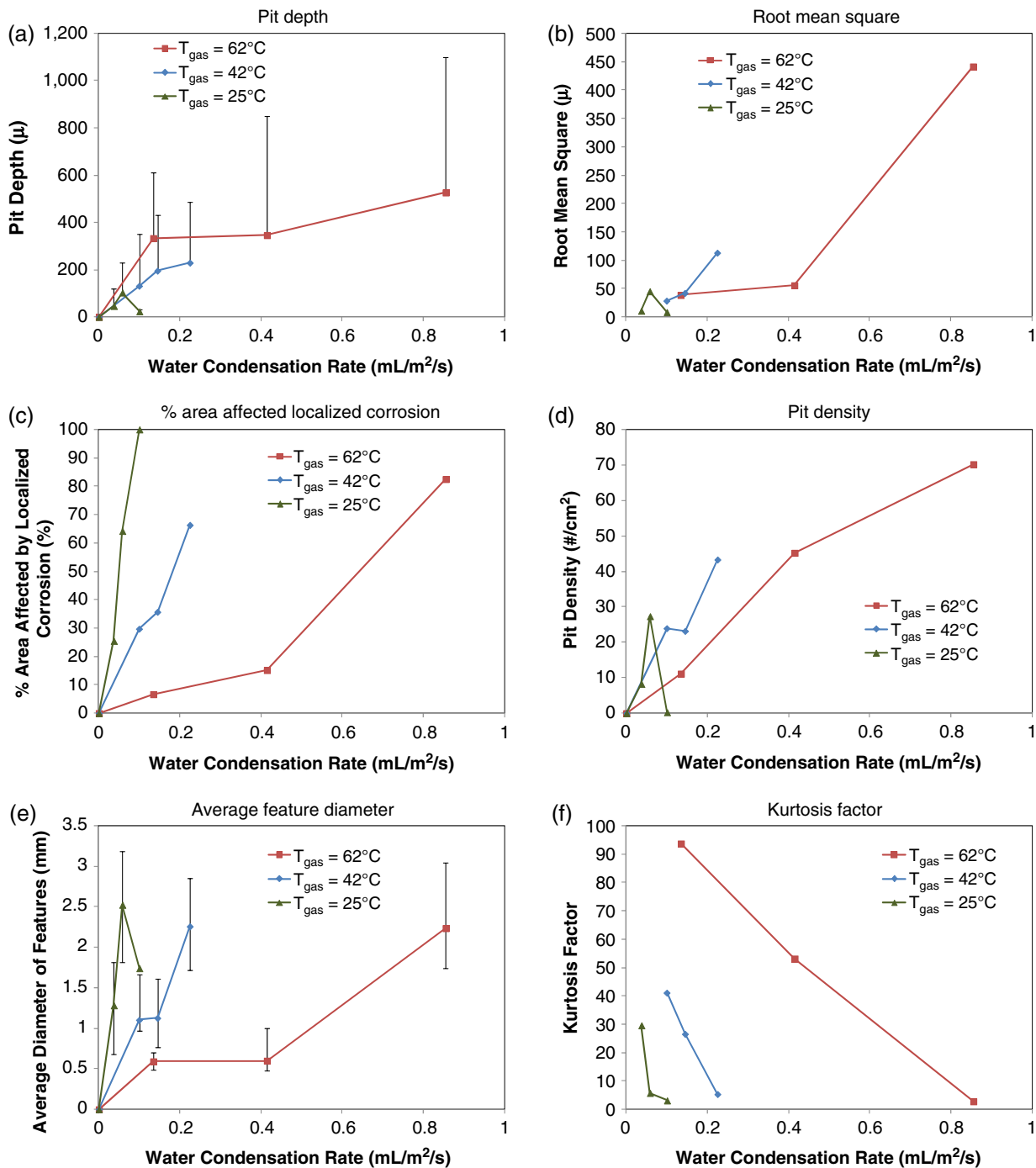


FIGURE 15. Influence of the gas temperature and the WCR. Summary of results.

the steel surface affected by localized corrosion (Figure 16[c] and [e]). Because the solution is more aggressive, pits seem to cluster more easily and mesa type attack is more wide spread. The decrease in pitting density with acetic acid (Figure 16[d]) is a result of the increase in feature size.

The presence of 1,000 ppm of undissociated acetic acid did not completely change the picture as

compared with the baseline test. However, the extent of the corrosion attack was more severe. This is to be expected as the presence of an additional weak acid in solution decreases the pH of the condensed water and acts as a buffer with regard to hydrogen ions and increases the solubility of FeCO₃. Average and maximum pits depths are also consequently higher in the presence of organic acid.

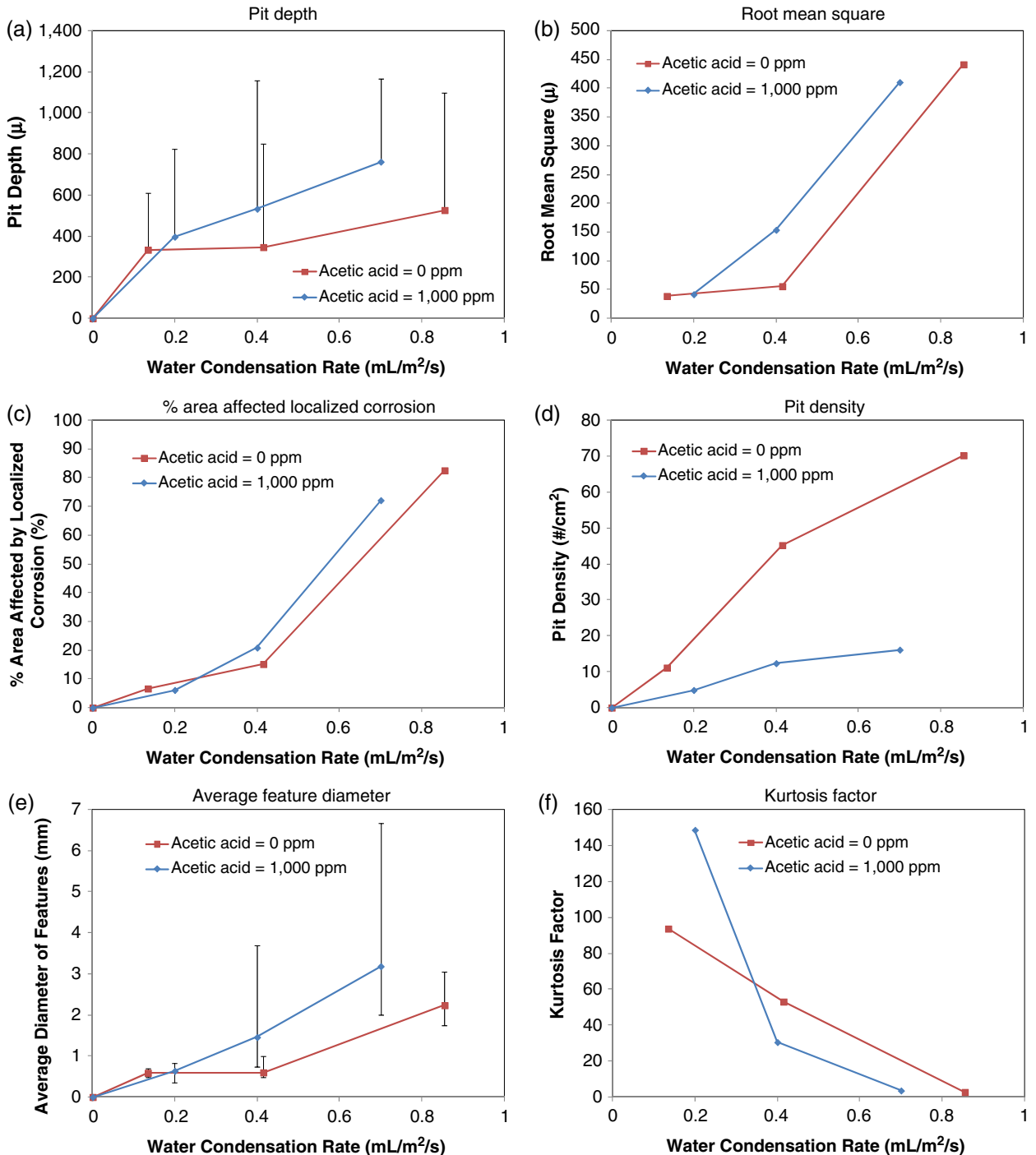


FIGURE 16. Influence of the acetic acid concentration and the WCR. Summary of results.

Part 2: Direct Observation of the Condensation Process

This section constitutes an investigation of the interaction between the presence of droplets of condensed water and the extent of the corrosion attack. The hypothesis is that, in dropwise condensation mode, the droplet will always tend to form at specific locations on the steel surface (broken corrosion product film

or location with higher surface roughness). These locations suffer from high condensed water renewal rate, inevitably leading to severe localized corrosion.

Direct Observation of the Presence of Droplets of Condensed Water — A number of experiments were performed in the newly developed flat slab test section in order to capture the interaction between the condensation process and the extent of the corrosion

attack. The in situ video camera was used to observe the condensation process. Only relatively low WCRs could be tested, as higher rates would lead the camera lens to be constantly obstructed by water.

A number of experiments were conducted, but the following section only presents the most relevant results related to three cases:

- Example A: Observation of the condensation process on a steel sample (Low WCR).
- Example B: Observation of the condensation process on a steel sample (medium WCR).
- Example C: Simulation of an artificial water trap on a steel insert.

Example A: In Situ Observation of the Condensation Process (low Water Condensation Rate) — A long-term TLC experiment lasting 43 d was performed in the TLC flow loop. The experimental conditions were as follows: P_T : 4.4 bars, pCO_2 : 4.2 bars, gas temperature: 62°C, WCR: 0.05 mL/m²/s, undissociated acetic acid: 1,000 ppm, gas velocity: 2 m/s. A API 5L X65 cylindrical sample was inserted into the “flat slab” test section at the beginning of the experiment once the test conditions were stable. One thousand parts per million of total acetic acid was introduced into the loop 2 h before the insertion of the weight loss samples. Pictures and video clips of the condensation process happening on the exposed sample were taken every 2 d to 3 d.

Figure 17 shows random pictures of the weight loss sample taken over the entire duration of the experiment. Because of technical limitations, only the upper part of the sample can be seen. Small droplets initially formed on the freshly polished surface of the sample, which eventually coalesced together and wetted the surface uniformly. After a few days of testing, a single large droplet could be seen on the right side of the picture. The rest of the surface was either covered

with smaller droplets or with a thinner film, while some part of the sample did not appear to be wetted at all. The condensation is a heterogeneous process strongly influenced by nucleation sites such as non-uniformity in the corrosion product scale. The droplet still seemed to always form at the same location on the steel surface. The large droplet went through the typical cycle of growth and fall. Another droplet would always replace it at the exact same location on the steel surface. The maximum droplet radius measured around 8 mm and the duration of the cycle “growth/removal” could reach 20 min to 60 min.

The sample was recovered at the end of the experiment and the corrosion product layer was identified as FeCO₃ through EDS analysis. On the area covered by the droplet, the crystals showed sharp edges and formed a dense layer (see Figure 18). Once the layer was removed, some evidence of localized corrosion could be seen with pits as deep as 220 μm. This corresponded to an average pitting rate over the 43 d of testing of around 1.8 mm/y, which is nine times higher than the uniform corrosion rate, measured at around 0.2 mm/y. However, the particular section of the sample that was continuously monitored and where a large droplet was continuously present did not show any clear evidence of localized corrosion. The maximum localized corrosion rate (if any) was measured at around 0.7 mm/y which is only 3.5 times higher than the uniform corrosion rate. No clear link could be made between the location of the droplet and the extent of the corrosion attack. This could be a result of the relatively low WCR in this test (WCR: 0.05 mL/m²/s).

Example B: In Situ Observation of the Condensation Process (Medium Water Condensation Rate) — Another experiment was performed in the flow loop. The experimental conditions were as follows: P_T : 4 bars, pCO_2 : 2.7 bars, Gas temperature: 59°C, WCR: 0.2 mL/m²/s,

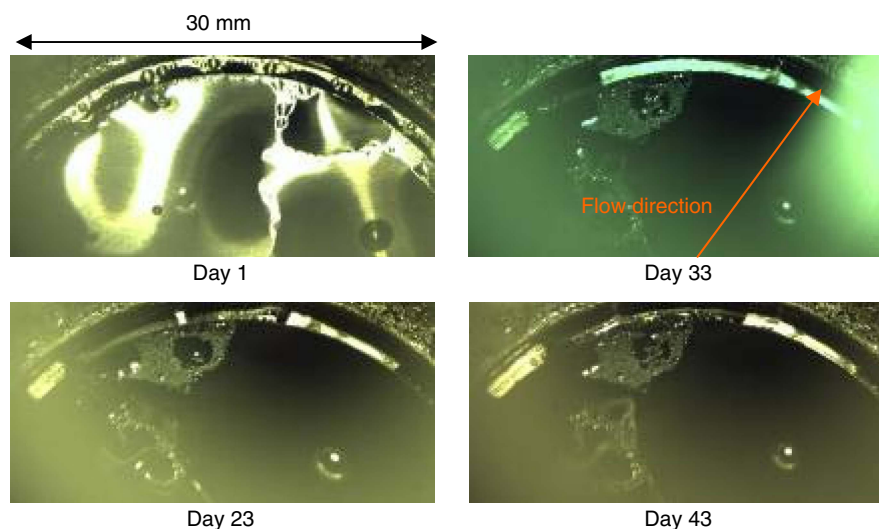


FIGURE 17. Localized corrosion test—Condensation process. A droplet of condensed water always forms at the same location.

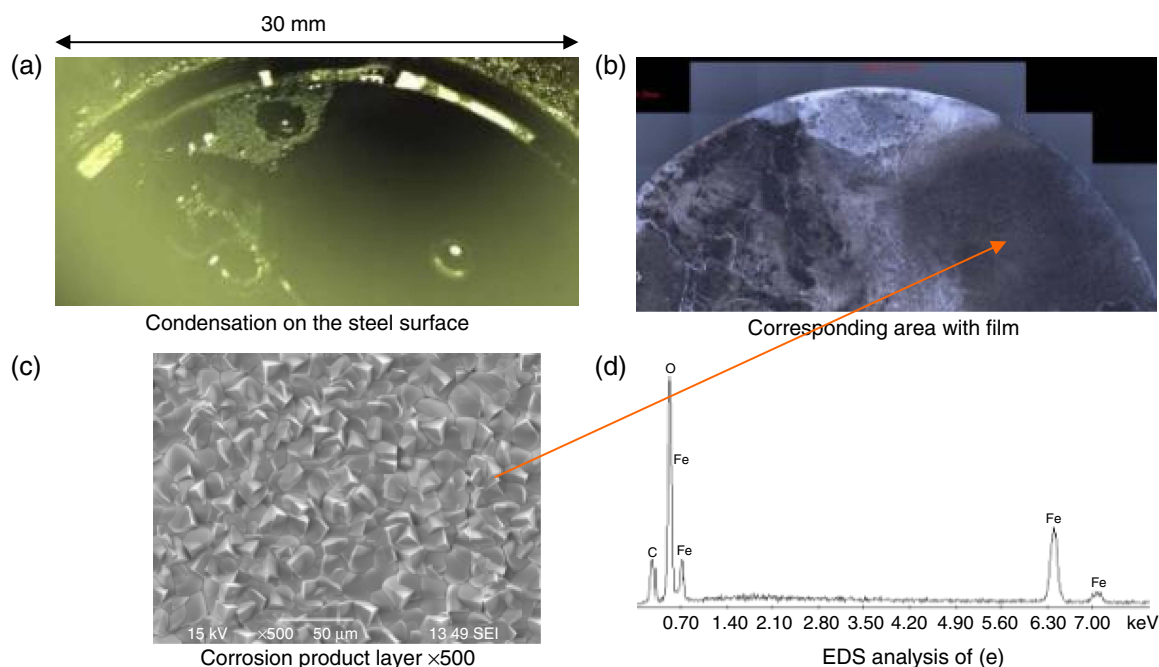


FIGURE 18. Surface analysis of the surface wetted by the droplet.

undissociated acetic acid: 1,000 ppm, gas velocity: 4 m/s. As in Figure 17, a large droplet was always present on the steel surface more or less at the same location on the sample.

Figure 19 shows the relative position of this droplet with regard to the localized corrosion analyzed after the end of the experiment. It seems that pits are located in a more or less random fashion with regard to the morphology of the water droplet. The extent of corrosion on the edges of the droplet, where the fresh corrosive condensed liquid is more quickly renewed, was not more severe than on the rest of the steel surface. It is also interesting to note that, even after the removal of the corrosion product layer using inhibited acid, the pits are still surrounded by a dark ring of what is believed to be remaining FeCO_3 . Although, the rest of the steel surface is easily cleaned, the corrosion product layer next to the pit seems to be much denser.

Example C: Artificial Water Trap — Another attempt to link condensation and corrosion process was made during the same long term test described in Example B. The small indentations (1.7 mm deep) were drilled on the upstream and downstream sections of the slab in order to develop artificial local areas where the condensed water would be trapped (Figure 20). The local WCRs were expected to be higher as a result of the lower steel thickness. However, the difference in WCR was neglected as most of the temperature drop happens at the gas/liquid interface and not through the liquid or the steel. The WCRs were set at $0.2 \text{ mL/m}^2/\text{s}$ and $0.7 \text{ mL/m}^2/\text{s}$ at the location of the two artificial traps, respectively.

Surface profile scans of the indentations were performed before the beginning of the tests (using molds) in order to document a reference depth. Surface profile scans were also run after the end of the test and after the removal of the corrosion product layer (Figure 21). No real difference in the extent of the corrosion attack could be seen between the artificial indentation and the surrounding area. The area exposed to a lower condensation rate suffered from the growth of small isolated pits. The area exposed to the highest condensation rate experienced extensive pitting, but the localized corrosion did not seem to be aggravated inside the artificial indentation.

Table 3 shows the evolution of the depth of the artificial indentation with time on both upstream and downstream sections. It appears that the indentation located on the section exposed to the low condensation rate did not grow at all. On the downstream cooled section (corresponding to a WCR of $0.7 \text{ mL/m}^2/\text{s}$), the depth of the indentation increased by $184 \mu\text{m}$, but that also corresponds to a somewhat lower corrosion rate (0.68 mm/y) than on the surrounding areas (3.63 mm/y). There was, therefore, no preferential corrosion inside the artificial indentations.

Part 3: Characteristics of Localized Features at the Top of the Line

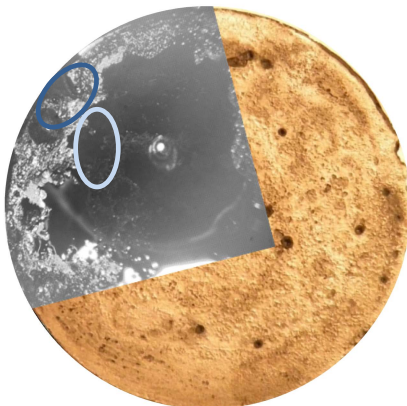
A flow loop experiment was performed with the intent of collecting information about localized corrosion characteristics. The experiment was performed using the flat slab equipped with corrosion probe



Picture of the sample before removal of the corrosion product layer



Picture of the sample after removal of the corrosion product layer



Picture of the droplet of condensed water super imposed on the sample steel surface after removal of the corrosion product layer

FIGURE 19. Interaction between corrosion product, condensation process and pitting.

ports.³⁰ The experimental conditions were as follows: P_T : 4.3 bars, pCO_2 : 4 bars, Gas temperature: 70°C, WCR: 0.4 mL/m²/s to 0.6 mL/m²/s, undissociated acetic acid: 0 ppm, gas velocity: 2.5 m/s, exposure time: 21 d, steel type: API 5L X65. The test conditions were selected for their aggressiveness, in order to ensure that large localized features would be created. The focus of this experiment was not to measure the actual corrosion rate but more to preserve steel

samples for further SEM, EDS, and XRD analysis. General observations on the morphology of localized corrosion features are made as follows based on the results of this experiment, but other comments are derived from experience gathered throughout the course of the present study.

Analysis of Localized Feature Characteristics — After the end of the experiment, the weight loss samples were visually inspected and the typical gray corrosion product layer was present on the metal surface. The surface coverage was largely uniform, but breakdown of the corrosion product layer could also be seen and be indicative of potential localized corrosion (Figure 22).

XRD analysis (Figure 22) clearly identified $FeCO_3$ as the sole component of the corrosion product layer present on the metal surface. No iron oxide could be detected, either by visual observation of the sample surface or by XRD analysis.

The SEM analysis (Figure 23) focused on several of the breakdown features and provided general information on the composition of the layer and morphology of the pits.

Some common characteristics of these breakdown features were as follows:

- The top layer of the corrosion product was comprised of tightly packed crystals of $FeCO_3$. The size of the crystals varied between 10 μm and 20 μm (Figure 23[c] and [e]).
- Several large breakdown features in the corrosion product layer were encountered. In almost all of the cases, a more amorphous phase, identified as Fe_3C , was present inside these breakdown features (Figure 23[d] and [f]).

After removal of the corrosion product layer, using inhibited acid, large localized corrosion features were visible and could be clearly correlated with the location of the $FeCO_3$ breakdown.

The sample was mounted in epoxy and cut in order to perform a cross sectional analysis of one of these breakdown features. The results are shown in Figures 24 through 26. Once again, several common characteristics are notable:

- A 20 μm to 70 μm thick $FeCO_3$ layer could clearly be seen on both sides of the localized feature, which could itself reach a depth close to 400 μm (Figure 24[a] and [b]).
- The features were quite wide and relatively flat bottomed. The actual pit was much larger than the layer breakdown would show.
- The pit was relatively empty. Often, the remainder of the $FeCO_3$ layer could be seen “hanging” on top of the pit, although there was nothing to support it.

Large amounts of $FeCO_3$ crystals were encountered on the side walls of the pits (Figure 25). $FeCO_3$ seemed to precipitate preferentially on already formed $FeCO_3$ crystals, rather than on the bare steel surface.

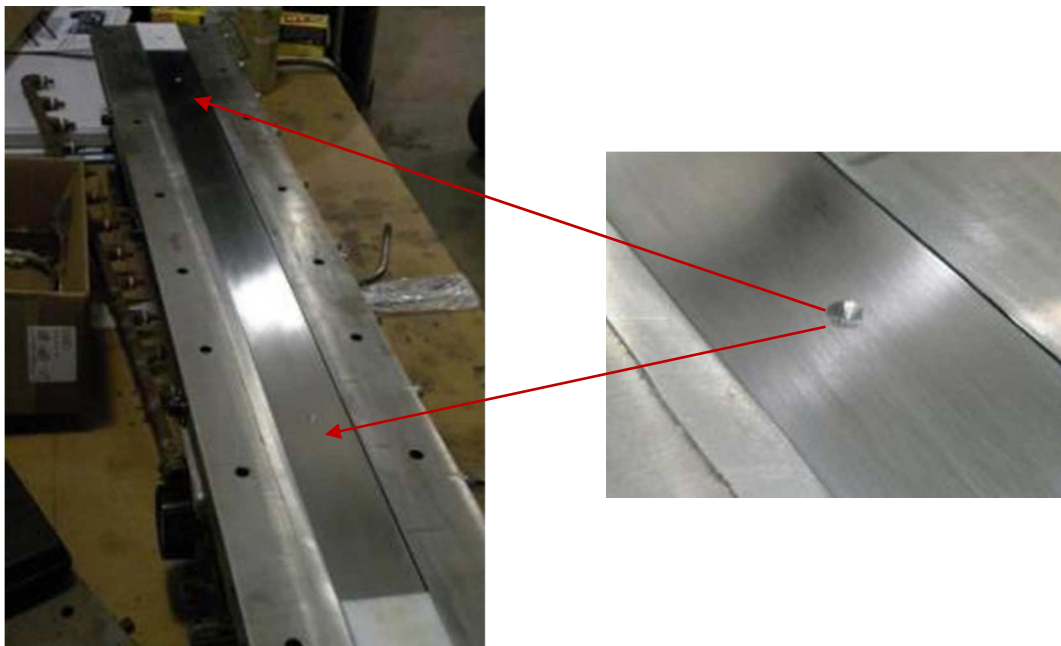


FIGURE 20. Artificial indentations created on the steel insert before the beginning of the test.

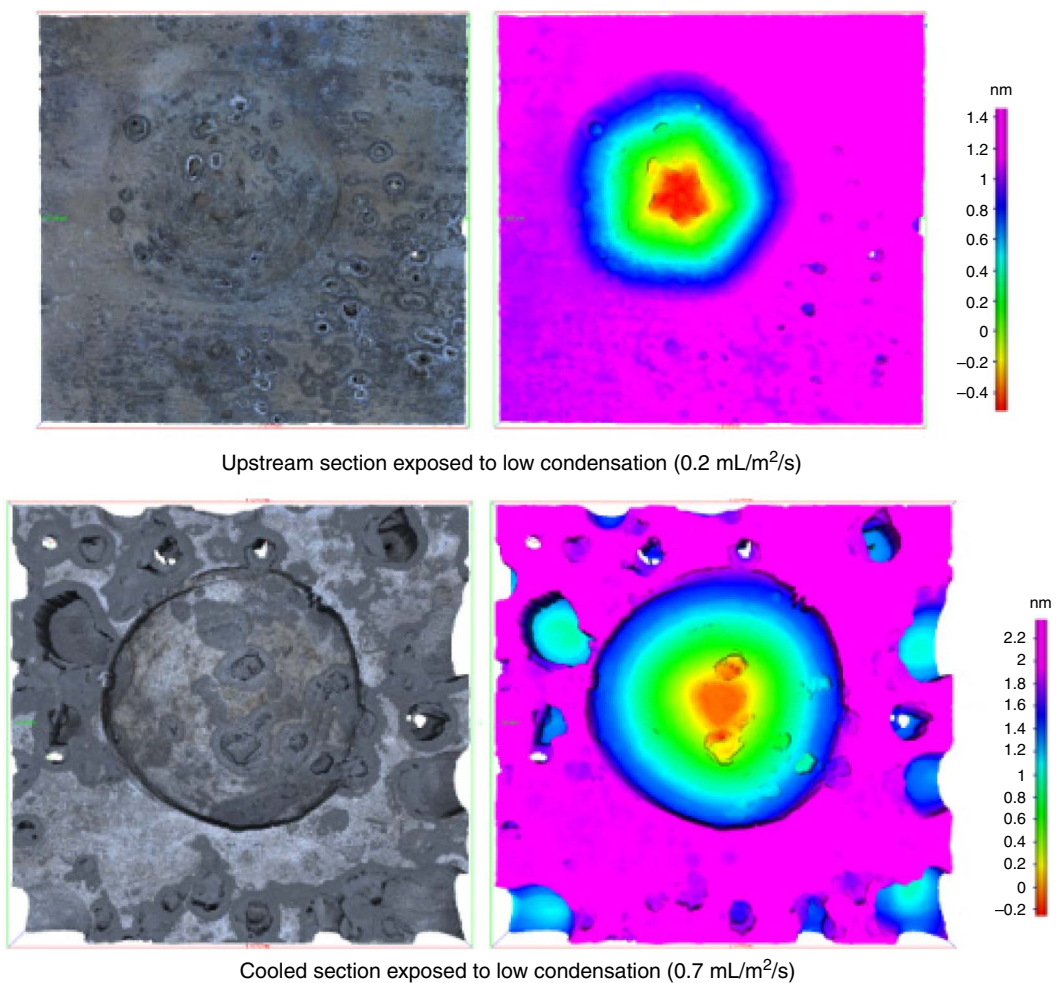


FIGURE 21. Morphology of the artificial indentation after the end of the experiment.

TABLE 3

Test No. 4: Corrosion Analysis on the Artificial Holes

	Initial Depth μm	Final Depth μm	Pit Growth μm	Pit Growth Rate mm/year	Average Pit Depth μm	Average Pitting Rate mm/year
Upstream section Low condensation rate	1842	1856	14	0.05	681	2.51
Downstream section High condensation rate	2193	2377	184	0.68	983	3.63

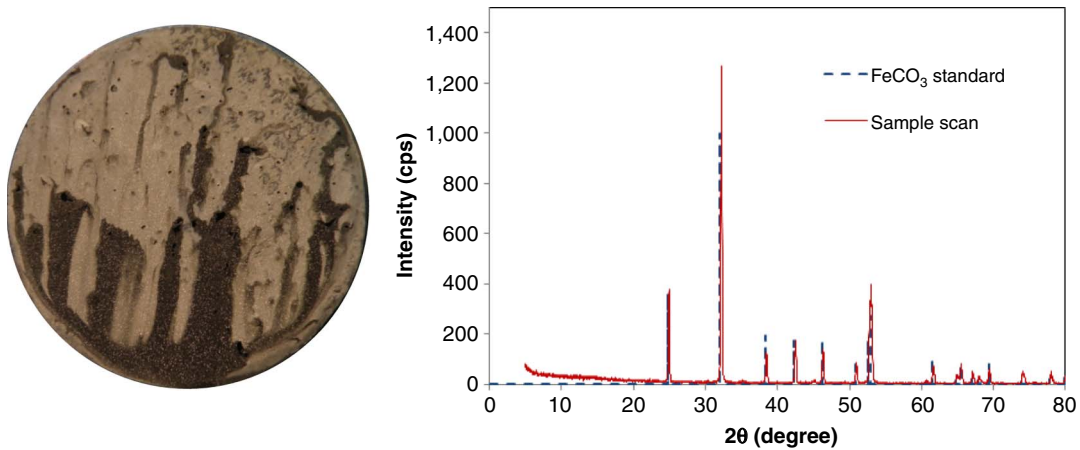


FIGURE 22. Weight loss sample with corrosion product layer (right) and XRD analysis identifying the presence of FeCO_3 (left).

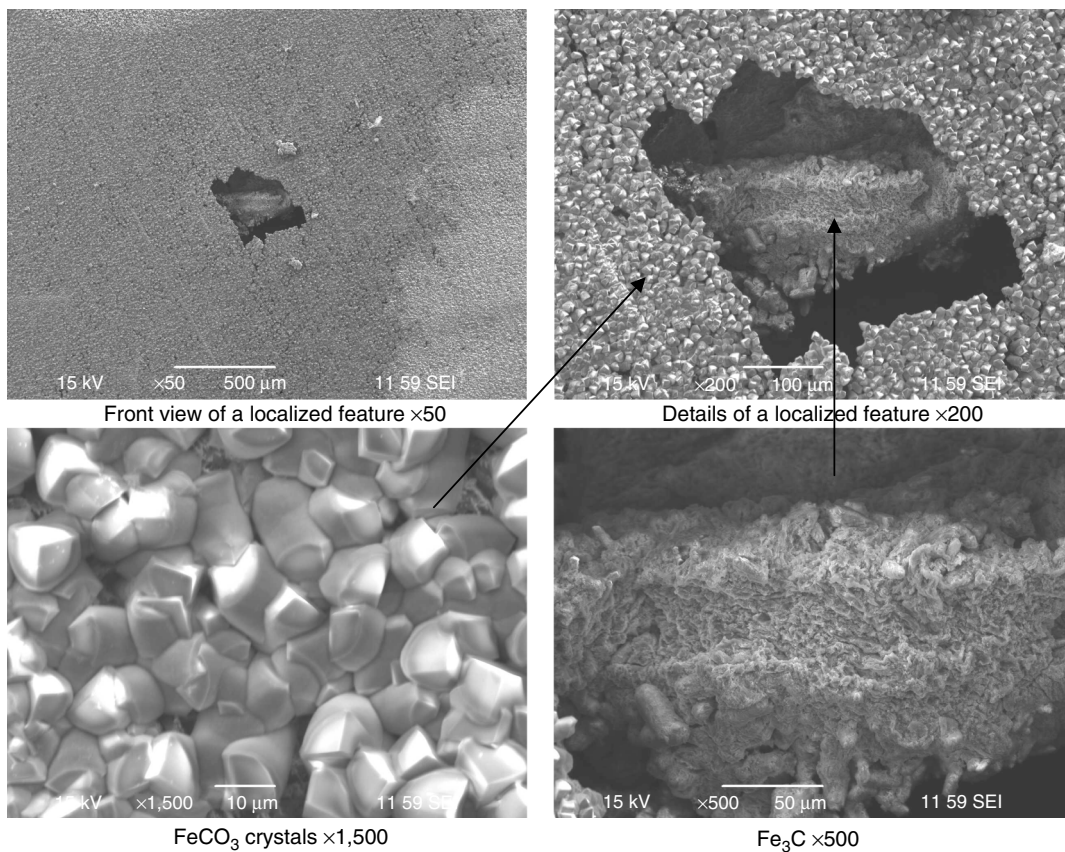


FIGURE 23. EDS analysis of the corrosion product layer and associated breakdowns.

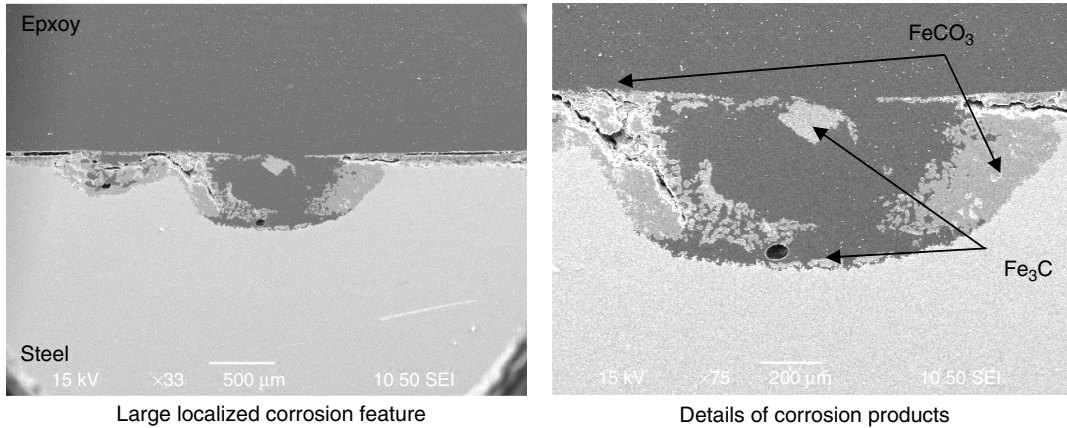


FIGURE 24. Cross-section analysis—Morphology of large localized features.

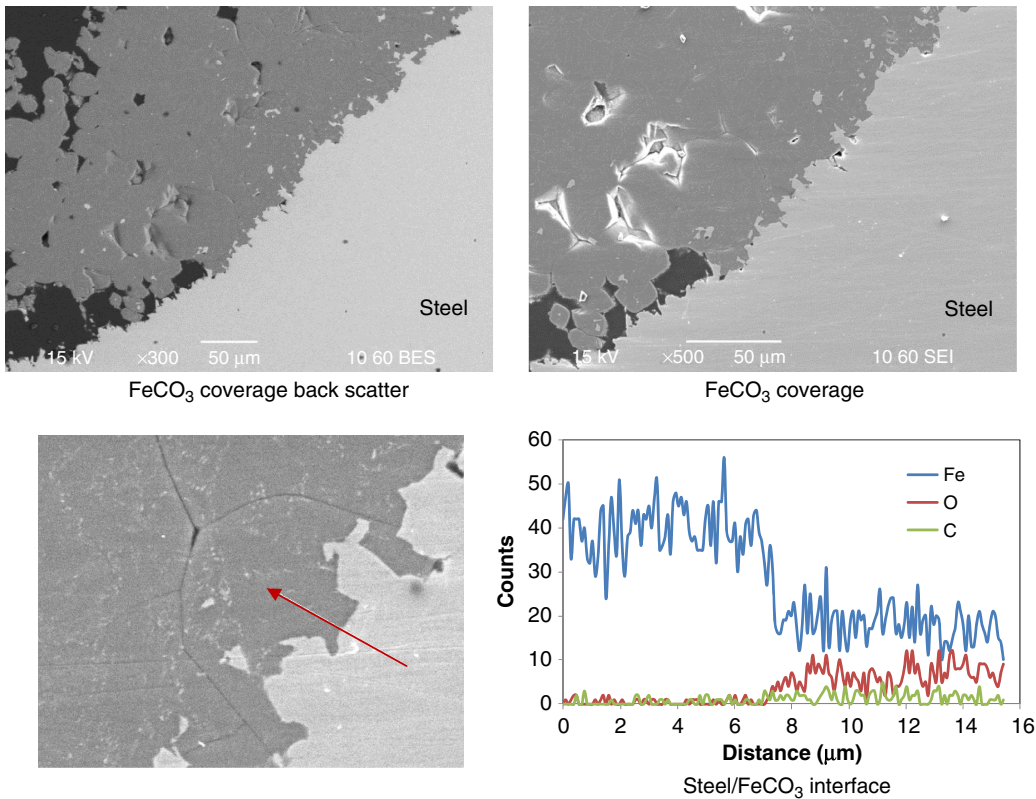


FIGURE 25. Cross-section analysis— FeCO_3 coverage on the side of the localized feature and EDS Line scan (along the red line).

This was especially true if the corrosion rate was high and the undermining effect considerable. On the areas well covered by FeCO_3 , the crystals were tightly packed and formed an effective mass transfer barrier. Pearlite lamellae were superimposed onto the FeCO_3 crystal network (Figure 25[d]). Fe_3C was identified at the bottom or at the center of the pit. This was not an indication that the pH inside the pit was acidic. It was, rather, an indication that FeCO_3 did not precipitate at that specific location (Figure 26). A line EDS

performed at the steel/ FeCO_3 interface could not confirm the presence of an iron oxide layer, contrary to what has been proposed elsewhere³²⁻³³ albeit using a more precise technique (transmission electron microscopy).

General comments can be made related to the properties of the FeCO_3 layer as follows:

Initiation of Localized Corrosion— In most of the TLC experiments performed, a very dense and tightly packed FeCO_3 layer formed on the metal surface and

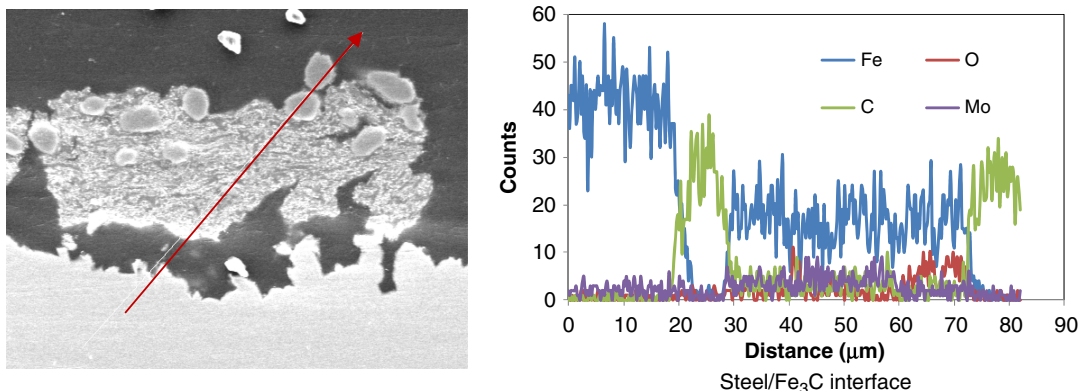


FIGURE 26. Cross-section analysis— Fe_3C coverage on the side of the localized feature and EDS Line scan (along the red line).

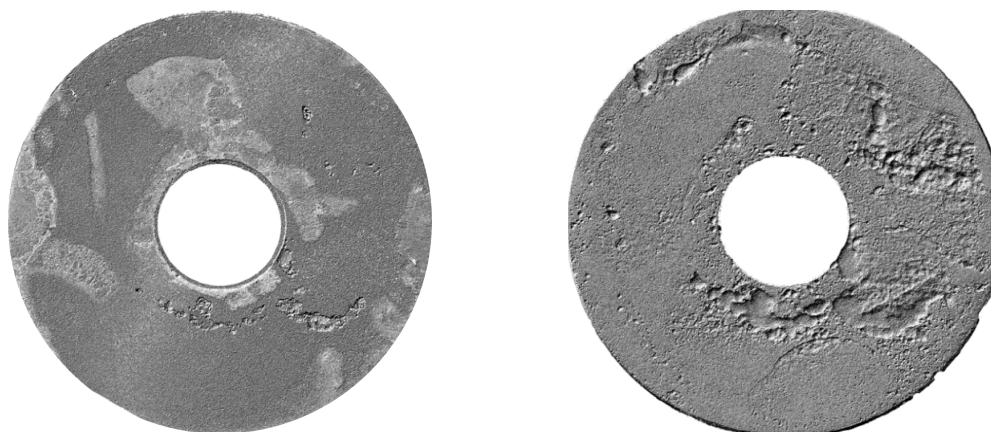
provided effective protection against corrosion. However, numerous breakdowns in the otherwise protective layer could be seen after long term exposure to the corrosive environment.

No localized corrosion was ever observed on the steel samples after short term exposure. However, there were signs that the FeCO_3 was not completely uniform on the entire metal surface.³⁰ The non-uniformity in the FeCO_3 coverage is mostly a result of the rate of water renewal on the steel surface, which constantly brings new, aggressively condensed water and alters the chemistry. Although pitting corrosion does not happen to any measurable extent on short term exposure, non-uniformity in the FeCO_3 coverage is visible and could lead to the initiation of localized corrosion later on.

Localized Corrosion Growth — Figure 27 shows the 3D surface profile performed before and after the removal of the corrosion product layer (Figure 27[a] and [b],

respectively). This experiment was performed over a 21-d period. Although breakdowns of the layer could clearly be seen, areas affected by high localized corrosion rates covered a much higher percentage of the surface. This shows that localized corrosion grew in depth but also underneath the corrosion product layer. This undermining effect could lead to the collapse of large portions of the FeCO_3 layer (Figure 28[a]).

Localized Corrosion Termination/Sustainability — Figure 28(b) presents a cross section of a TLC localized feature whose bottom part seems to be well covered by an FeCO_3 layer and, therefore, protected against further corrosion. This shows that not all of the TLC features remain “active” throughout the exposure to the corrosive environment. The reason behind such behavior is unclear but could be a result of mass transfer limitation, which would make FeCO_3 precipitation more likely at the bottom of deep and narrow



3D profile before removal of the corrosion product layer

3D profile before removal of the corrosion product layer

FIGURE 27. Localized corrosion features growth underneath FeCO_3 layer. $T=70^\circ\text{C}$, WL X65, $\text{HAc}=0$ ppm, $\text{WCR}=1$ $\text{mL/m}^2/\text{s}$, Exposure time = 21 d.

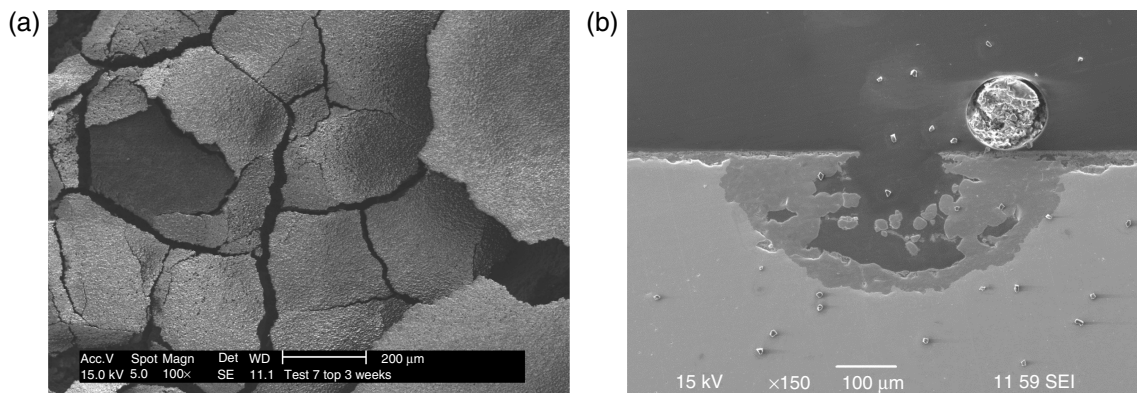


FIGURE 28. FeCO_3 top layer collapsing (a) and FeCO_3 layer regaining coverage on the metal surface (b) $T = 70^\circ\text{C}$, WL X65, $\text{HAc} = 1,000$ ppm, $\text{WCR} = 1$ $\text{mL/m}^2/\text{s}$, Exposure time = 21 d.

localized features, while other, shallower pits would continue to grow.

Comments on TLC stabilization — The characteristics of the TLC features (large, flat-bottomed, and layer-free) and the fact that the pitting rate is usually comparable to bare steel corrosion rate³⁰ point out that the severity of the TLC attack should be controlled by the corrosiveness of the environment and the WCR. Any galvanic effect between the bare steel and the surrounded layer-covered surface is not likely to be significant. Placed in the context of a pipeline environment subject to TLC, metal loss is consequently expected to occur continuously over the production life, assuming no dramatic change in the operating conditions.

However, the experimental observations presented in this study do show that the pit penetration rate seems to decrease with time, and this appears to be consistent with the notion of TLC stabilization introduced earlier.⁹ Some experimental work has been performed to explain how the conditions at the bottom of a pit become less corrosive as localized corrosion progresses.²⁸⁻²⁹ This could explain why some TLC localized features may cease to progress in depth after a period of time.

Actual stabilization of TLC features, however, cannot be fully explained theoretically. Once these pits become wide enough, the mass transfer limitations associated with TLC stabilization should no longer hold. In addition, the continuous dilution of ferrous ions due to condensation must be matched with a corresponding source of ferrous ions from corrosion or layer dissolution in order to maintain FeCO_3 saturation inside the droplet. Consequently, the metal loss rate, averaged over long periods of time, must be constant as long as the operating conditions (i.e., condensation rate) do not change. Experimental validation of TLC stabilization is difficult and would require very long and impractical testing time. In the author's view, whether TLC stabilization is a real phenomenon or

the result of changing operating conditions remains a fundamental question.

CONCLUSIONS

❖ Part 1: Corrosion Study

A new experimental setup (carbon steel inserts in flat slab) was developed to improve the quality of the experimental data. The new set of experiments was successful in simulating TLC without obvious edge effects and in capturing the effect of the condensation rate. Localized corrosion could be very clearly observed on the steel surface and correlated to the condensation rate and the gas temperature.

- Pitting/mesa corrosion is strongly related to the level of condensation applied to the steel section.
- On the thermally insulated areas, localized corrosion is marginally observed but does not grow with time after the first months of exposure.
- On the cooled section, pits still seem to be growing in depth with time and also form clusters.
- In the presence of undissociated acetic acid, the extent of the corrosion attack was much more severe compared to previous results obtained without acetic acid. In particular, the condensation rate did not seem to have a strong effect on the maximum depth of the corrosion features.
- These observations are in agreement with field observations of TLC.

❖ Part 2: Direct Observation of the Condensation Process

It is clear from the experiments performed that, once the initial nucleation/growth/coalescence cycle is completed, larger droplets always seem to form at the same location on the steel surface. Once they reach their

maximum size, they leave the location (either by falling or sliding along the pipe), leaving a thin liquid layer behind, where condensed water then accumulates preferentially. The steel surface between large droplets is usually wetted by a thin, continuous liquid film. However, the presence or absence of a large droplet on the steel surface cannot be correlated directly to the extent of corrosion occurring underneath, as follows:

- In cases of high WCR, severe localized corrosion happens everywhere on the steel surface, irrespective of where the large droplets are. Underneath the droplet, the corrosion features are larger but seem to progress at the same rate as anywhere else on the steel surface.
- In cases of low condensation rate, isolated pitting could still be observed on the steel surface, but no correlation with the presence of a large droplet could be validated.
- Artificial “water traps” do not promote higher localized corrosion.
- The extent of corrosion is controlled by the rate of water condensation and the overall aggressiveness of the environment (CO₂, acetic acid).

❖ Part 3: Characteristics of localized features at the top of the line

TLC localized features can be wide and relatively flat bottomed. The actual pit can be significantly larger than the corresponding FeCO₃ layer breakdown seen on top of it before the removal of the layer. The pits are relatively empty, and layers of FeCO₃ can be seen “hanging” on top of the pit, although there is little to mechanically support them. Large amounts of FeCO₃ crystals are encountered on the side walls of the pits while the bottom part is bare steel. FeCO₃ grows preferentially on already formed FeCO₃ crystals, rather than on the steel surface. Large pieces of FeCO₃ are identified at the bottom or at the center of the pit. This is not an indication that the pH inside the pit is acidic. It is, rather, an indication that FeCO₃ did not precipitate at that specific location.

ACKNOWLEDGMENTS

The author would like to acknowledge the support of the sponsors of the TLC Joint Industry Project at Ohio University.

REFERENCES

1. Y. Gunaltun, D. Supriyataman, A. Jumakludin, “Top of the Line Corrosion in Multiphase Gas Line. A Case History,” CORROSION 1999, paper no. 36 (Houston, TX: NACE, 1999).
2. Y. Gunaltun, D. Larrey, “Correlation of Cases of Top of the Line Corrosion with Calculated Water Condensation Rates,” CORROSION 2000, paper no. 71 (Houston, TX: NACE, 2000).
3. Y. Gunaltun, R. Piccardino, D. Vinazza, “Interpretation of MFL and UT Inspection Results in Case of Top of Line Corrosion,” CORROSION 2006, paper no. 6170 (Houston, TX: NACE, 2006).
4. G. Bourriot, “Top of Line Corrosion Cases at Total E&P Netherlands,” 2nd TOL Corrosion Conference 2009 (Bangkok: PTTEP, 2009).
5. D. Hinkson, G. Peck, “Field Assessment and Verification of Organic Acid Speciation for Corrosion Risk Assessment,” CORROSION 2010, paper no. 10100 (San Antonio, TX: NACE, 2010).
6. J.R. Piccardino, M. Stuvik, Y. Gunaltun, T. Pornthep, “Internal Inspection of Wet Gas Line Subject to Top of Line Corrosion,” CORROSION 2004, paper no. 4354 (Houston, TX, 2004).
7. M. Thammachart, Y. Gunaltun, S. Punpruk, “The Use of Inspection Results for the Evaluation of Batch Treatment Efficiency and the Remaining Life of the Pipelines Subjected to Top of Line Corrosion,” CORROSION 2008, paper no. 8471 (New Orleans, LA: NACE, 2008).
8. Y. Gunaltun, L. Payne, “A New Technique for the Control of Top of Line Corrosion: TLCC-PIG,” CORROSION 2003, paper no. 3344 (Houston, TX: NACE, 2003).
9. U. Kaewpradap, M. Singer, S. Nestic, S. Punpruk, “Top of the Line Corrosion—Comparison of Model Predictions with Field Data,” CORROSION 2012, paper no. 1449 (New Orleans, LA: NACE, 2012).
10. U. Kaewpradap, “Validation of Top of the Line Corrosion Prediction Model Using Laboratory and Field Measurements” (Master’s Thesis, Chemical and Bio-molecular Engineering Department, Ohio University, 2012).
11. Y. Gunaltun, S. Punpruk, M. Thammachart, T. Pornthep, “Worst-Case TLC: Cold Spot Corrosion,” CORROSION 2010, paper no. 10097 (San Antonio, TX: NACE, 2010).
12. Y. Gunaltun, M. Thammachart, M. Singer, S. Nestic, S. Punpruk, U. Kaewpradap, “Progress in the Prediction of Top of the Line Corrosion and Challenges to Predict Corrosion Rates Measured in Gas Pipeline,” CORROSION 2010, paper no. 10093 (San Antonio, TX: NACE, 2010).
13. S. Olsen, A. Dugstad, “Corrosion Under Dewing Conditions,” CORROSION 1991, paper no. 472 (Houston, TX: NACE, 1991).
14. B.F.M. Pots, E.L.J.A. Hendriksen, “CO₂ Corrosion Under Scaling Conditions—The Special Case of Top-of-the-Line Corrosion in Wet Gas Pipelines,” CORROSION 2000, paper no. 31 (Houston, TX: NACE, 2000).
15. F. Vitse, “Experimental and Theoretical Study of the Phenomena of Corrosion by Carbon Dioxide Under Dewing Conditions at the Top of a Horizontal Pipeline in Presence of a Non-condensable Gas” (Ph.D. diss., Russ College of Engineering, Department of Chemical Engineering, Ohio University, Athens, OH, 2002).
16. F. Vitse, S. Nestic, Y. Gunaltun, D. Larrey de Torreben, P. Duchet-Suchaux, *Corrosion* 59, 12 (2003), p. 1075-1084.
17. F. Vitse, K. Alam, Y. Gunaltun, D. Larrey de Torreben, P. Duchet-Suchaux, “Semi-empirical Model for Prediction of the Top-of-the-Line Corrosion Risk,” CORROSION 2002, paper no. 2245 (Houston, TX: NACE, 2002).
18. M. Singer, D. Hinkson, Z. Zhang, H. Wang, S. Nestic, *Corrosion* 69, 7 (2013), p. 719-735.
19. C. Mendez, M. Singer, A. Camacho, S. Hernandez, S. Nestic, “Effect of Acetic Acid, pH and MEG on CO₂ Top of the Line Corrosion,” CORROSION 2005, paper no. 5278 (Houston, TX: NACE, 2005).
20. R. Nyborg, A. Dugstad, “Top of the Line Corrosion and Water Condensation Rates in Wet Gas Pipelines,” CORROSION 2007, paper no. 7555 (Nashville, TN: NACE, 2007).
21. J.L. Crolet, M. Bonis, “The Role of Acetate Ions in CO₂ Corrosion of Carbon Steel,” CORROSION 1983, paper no. 160 (Houston, TX: NACE, 1983).
22. P. Okafor, S. Nestic, *Chem. Eng. Commun.* 194, 2 (2007), p. 141-157.
23. Z. Zhang, D. Hinkson, M. Singer, H. Wang, S. Nestic, *Corrosion* 63, 11 (2007), p. 1051-1062.
24. A. Rotimi, R.A. Ojifinni, C. Li, “A Parametric Study of Sweet Top of the Line Corrosion in Wet Gas Pipelines,” CORROSION 2011, paper no. 11331 (Houston, TX: NACE, 2011).
25. D. Hinkson, Z. Zhang, M. Singer, S. Nestic, *Corrosion* 66, 4 (2010), p. 045001-045001-8.
26. T. Pojtanabuntoeng, M. Singer, S. Nestic, “Water/Hydrocarbon Co-condensation and the Influence on Top-of-the-Line Corrosion,” CORROSION 2011, paper no. 11330 (Houston, TX: NACE, 2011).
27. T. Pojtanabuntoeng, M. Singer, S. Nestic, “Top-of-the-Line Corrosion in the Presence of Hydrocarbon Co-condensation in Flowing Condition,” CORROSION 2012, paper no. 1534 (New Orleans, LA: NACE, 2012).

28. J. Amri, E. Gulbrandsen, R.P. Nogueira, *Electrochem. Commun.* 10, 2 (2008), p. 200-203.
29. J. Amri, E. Gulbrandsen, R.P. Nogueira, *Corrosion* 66, 3 (2010), p. 035001-035001-7.
30. M. Singer, "Study and Modeling of the Localized Nature of Top of the Line Corrosion" (Ph.D. diss., Russ College of Engineering, Department of Chemical Engineering, Ohio University, Athens, OH, 2013).
31. ASTM G1-03, "Standard Practice for Preparing, Cleaning and Evaluating Corrosion Test Specimens" (Philadelphia, PA: ASTM, 2009), p. 17-23.
32. J. Han, D. Young, H. Colijn, A. Tripathi, S. Nescic, *Ind. Eng. Chem. Res.* 48, 6 (2009), p. 6296-6302.
33. W. Li, B. Brown, D. Young, S. Nescic, *Corrosion* 70, 3 (2014), p. 294-302.